MNRAS **000**, 1–?? (2019) Preprint 13 May 2019 Compiled using MNRAS LATEX style file v3.0

unWISE Coadds: The Five-year Data Set

A. M. Meisner,[1⋆] D. Lang,[2] E. F. Schlafly[3] and D. J. Schlegel[3]
[1] *National Optical Astronomy Observatory, 950 N. Cherry Ave., Tucson, AZ 85719, USA*
[2] *Perimeter Institute, 31 Caroline Street North, Waterloo, ON, N2L 2Y5, Canada*
[3] *Lawrence Berkeley National Laboratory, Berkeley, CA, 94720, USA*

13 May 2019

ABSTRACT
We present full-sky coadded maps created by uniformly combining the first five years of Wide-field Infrared Survey Explorer (WISE) and NEOWISE imaging at 3.4μm (W1) and 4.6μm (W2). By incorporating both pre-hibernation WISE exposures from 2010-2011 and the first four years (2013-2017) of post-hibernation exposures from the NEOWISE-Reactivation mission, we are able to provide W1/W2 coadds that span a 15× longer time baseline and are substantially deeper than the standard AllWISE data products. Our new five-year "full-depth" coadds now represent the deepest ever all-sky maps at 3−5μm, permitting detection of sources ∼2× (∼0.7 mag) fainter than AllWISE at 5σ significance. We additionally present an updated set of "time-resolved" W1/W2 coadds, which separately stack each of ∼10 sky passes at each inertial sky location, enabling motion and variability measurements for faint infrared sources over a long ∼7.5 year time baseline. We highlight new processing improvements relative to our previous "unWISE" coadd releases, focusing on astrometric calibration and artifact flagging. The deep WISE stacks presented here are already being used to perform target selection for the Dark Energy Spectroscopic Instrument (DESI), and our full-sky coadded WISE/NEOWISE products will be key precursor data sets for upcoming wide-field infrared missions including SPHEREx and NEOCam.

Key words:
atlases — infrared: general — methods: data analysis — surveys — techniques: image processing

1 INTRODUCTION

In the coming years, an exciting array of space-based infrared astronomy missions are expected to launch, including SPHEREx (Doré et al. 2018), JWST (Gardner et al. 2006), Euclid (Racca et al. 2016), WFIRST (Spergel et al. 2015) and NEOCam (Mainzer et al. 2015). For the purposes of forecasting/simulating the data sets that will be obtained by these projects, and to select optimal targets for their pointed observations, it is critical to fully process and analyze existing all-sky infrared imaging.

Launched in late 2009, the Wide-field Infrared Survey Explorer (WISE; Wright et al. 2010) is a unique and unrivaled source of sensitive full-sky imaging in the mid-infrared. WISE has now provided the best ever all-sky images over the 3−22μm wavelength range, in four broad channels labeled W1 (3.4μm), W2 (4.6μm), W3 (12μm) and W4 (22μm). The WISE sensitivity is orders of magnitude better than that of its predecessor, the Infrared Astronomical Satellite (IRAS; Wheelock et al. 1994).

The WISE satellite's original objectives were primarily to study the most infrared-luminous galaxies in the Universe and identify extremely cold members of the Sun's local Galactic neighborhood. However, by now, more than 80% of WISE data at W1 and W2 has been acquired as part of the NEOWISE mission extension (Mainzer et al. 2011, 2014). NEOWISE is tasked with finding and characterizing asteroids, so the mission itself does not produce coadded data products of the sort that would maximize the value of its vast archive of raw imaging for Galactic and extragalactic astrophysics.

As a result, we have been undertaking a wide-ranging archival data analysis program to repurpose all publicly available W1/W2 data ever acquired for astrophysics beyond the solar system. This effort begins by uniformly stacking all WISE and NEOWISE single exposure data, with our data products referred to as "unWISE" coadds (Lang 2014). Our unWISE coadds have already provided the deepest ever full-sky maps (Meisner et al. 2017a,b, 2018a), source catalogs

⋆ ameisner@noao.edu

(Schlafly et al. 2019), and proper motion measurements[1] at 3−5μm. The Dark Energy Spectroscopic Instrument (DESI) pre-imaging surveys (Dey et al. 2019) have also provided forced photometry of our unWISE coadds for more than 1 billion optically selected sources over ∼1/3 of the sky (Lang et al. 2016).

Still, yet more single-exposure NEOWISE data remains to be incorporated into our analysis. Here, we update our unWISE coadd data set to include the fourth year of NEOWISE-Reactivation (NEOWISER; Mainzer et al. 2014) exposures gathered throughout 2017. In combination with existing WISE/NEOWISE data, this allows us to create yet deeper full-sky maps at 3−5μm and extend the time baseline to 7.5 years for proper motion and variability measurements based on epochal unWISE coadds (Meisner et al. 2018d,c). For this new "five-year" unWISE coadd data release, we have also implemented a number of processing improvements, particularly with regard to astrometric calibration and artifact flagging.

In §2 we briefly summarize the relevant WISE/NEOWISE mission characteristics and timeline. In §3 we describe the input data used to build our five-year unWISE coadds. In §4 we review key aspects of the unWISE data products in relation to those published by the WISE/NEOWISE teams. In §5 we provide details of the five-year unWISE coaddition process and results. In §6 we describe our astrometric recalibration of the five-year unWISE coadds using Gaia DR2 (Gaia Collaboration et al. 2018). In §7 we give a high-level summary of the improved artifact flagging we have implemented, with full details deferred to Appending A. In §8 we discuss the validation of our five-year unWISE coadds. In §9 we describe the five-year unWISE coadd data release. We conclude in §10.

2 WISE OVERVIEW

WISE is a 40 cm telescope aboard a satellite in a ∼95 minute low-Earth orbit. After launching in late 2009, WISE surveyed the entire sky in all four of its channels (W1-W4) during the first half of 2010. In the latter half of 2010, the reddest two channels (W3 and W4) became unusable due to cryogen depletion. Nevertheless, the WISE satellite continued surveying in W1 and W2 until early 2011 as part of the NEOWISE mission (Mainzer et al. 2011). In 2011 February, WISE was placed into hibernation for approximately 33 months, during which time it was not conducting astronomical observations. In 2013 December, WISE recommenced surveying in the available W1 and W2 bands, and has continued doing so ever since thanks to the NEOWISER mission extension (Mainzer et al. 2014). The very high W1/W2 data quality has remained essentially unchanged over the 9+ year timespan over which observations have been acquired in these two bands. The WISE angular resolution in W1 and W2 is ∼6″. WISE scans in great circles near solar elongation of 90°, with a typical sky region being observed over a $\gtrsim$1 day time period (referred to as a "visit") once every six months, during which time $\gtrsim$12 single-exposure images per band are acquired. Very close to the ecliptic poles, the WISE time coverage becomes essentially continuous, with one exposure available during nearly every ∼95 minute orbit.

[1] https://catwise.github.io/

3 WISE/NEOWISE DATA

The NEOWISER mission publicly releases single-exposure images and catalogs, but no coadded data products. Therefore, the W1/W2 single-exposure calibrated ("L1b") images provided by the WISE/NEOWISE teams represent the starting point of our unWISE coaddition processing. We begin by downloading all L1b images from the first five years of WISE observations: 13 months of pre-hibernation W1/W2 imaging plus the first four annual NEOWISER L1b data releases. These data have acquisition dates spanning from 2010 January 7 to 2017 December 13. This full set of archival W1/W2 single-exposure images constitutes a large volume of data: ∼13.1 million single-exposure images in each of two bands, totaling 175 terabytes. We note that a fifth year of post-reactivation W1/W2 single-exposure images recently became available on 2019 April 11 as part of the fifth annual NEOWISER data release, but we have not yet incorporated this most recent year of imaging into our unWISE coadds – doing so will be the subject of future work.

4 UNWISE COADD OVERVIEW

There are two lines of coadded full-sky WISE data products available: the AllWISE Source Catalog and Atlas stacks provided by the WISE/NEOWISE team (Cutri et al. 2013), and our unWISE coadds/catalogs. A major limitation of AllWISE for the W1/W2 bands is that it only incorporates the roughly one year of pre-hibernation WISE imaging, which now represents just a small fraction of the presently available data in these two bands. On the other hand, unWISE has been systematically incorporating all W1/W2 data, both pre-hibernation and post-reactivation, as NEOWISER continues issuing its annual single-exposure data releases (Meisner et al. 2017a,b, 2018d,a,c). Prior to the present work, the most recent set of unWISE coadds incorporates a total of four years of single-exposure W1/W2 data (pre-hibernation imaging plus the first three years of post-reactivation exposures).

Another important point of contrast is that the AllWISE Atlas stacks are intended to be used primarily for performing source detection, and have therefore been in effect "blurred" by the WISE PSF. On the other hand, unWISE uses Lanczos interpolation when reprojecting the single-exposure L1b images in order to retain the native WISE resolution; this yields coadds that are unblurred and optimized for forced photometry (Lang 2014).

There are two flavors of unWISE coadds: "full-depth" and "time-resolved". The full-depth unWISE coadds simply stack together all available W1/W2 single-exposure images at each sky location to produce the deepest possible static sky maps. On the other hand, our "time-resolved" unWISE coadds bin the exposures at each sky location into a series of six-monthly visits, with typically $\gtrsim$12 exposures stacked together per band per visit. Full details of this time-slicing procedure are provided in §3.2 of Meisner et al. (2018d). The

time-resolved unWISE coadds therefore provide a means of measuring long-timescale (several days to ∼8 years) variability and motion for faint sources far below the single-exposure detection limit (e.g., Kuchner et al. 2017; Ross et al. 2018; Stern et al. 2018), with the effects of fast transients such as cosmic rays and satellite streaks dramatically suppressed. Because the present work incorporates five years of W1/W2 data, our outputs typically include 10 coadded epochs per band at each sky location, spanning a 7.5 year time baseline.

unWISE coadds onto a set of 18,240 1.56°×1.56° 'tile' footprints each identified by a unique string `coadd_id` value, which encodes the location of the tile center. For example, the unWISE tile centered at $(\alpha, \delta) = (149.7485°, 1.51444°)$ has `coadd_id` = 1497p015. The unWISE tile centers and orientations are chosen to match those of the AllWISE Atlas stacks. unWISE coadds adopt the native W1/W2 single-exposure pixel scale of 2.75″/pixel, making each unWISE coadd image 2048×2048 pixels in size. The unWISE coadd images are in units of Vega nanomaggies.

5 FIVE-YEAR UNWISE COADDITION

5.1 Photometric calibration

Before proceeding to coadd the five years of L1b images downloaded, we begin by computing a custom photometric zero-point for each W1/W2 exposure so as to place all exposures on the most uniform possible relative photometric calibration. Per-exposure zero-points are needed to provide the multiplicative rescaling of each L1b image during unWISE coaddition. In brief, we measure the zero-point variation in each band in day-long intervals using repeat observations of stars near the ecliptic poles. We find that this procedure better maps out zero-point variations with time than does the per-exposure zero-point provided by the `MAGZP` keyword in each exposure's L1b header. Full details of our relative photometric calibration methodology can be found in §4 of Meisner et al. (2017a). Figure 1 shows the results of our photometric zero-point calibration as applied to the fourth year of NEOWISER exposures newly added to our coadds in this work.

5.2 Overview of five-year coaddition results

We ran the unWISE coaddition code without substantive modifications relative to the most recent algorithmic updates described in Meisner et al. (2017b) and Meisner et al. (2018d), but now employing five years of W1/W2 single-exposure imaging, which is a larger quantity of raw data than previously used for any full-sky unWISE coadd processing. The following subsections provide a big-picture overview of the full-sky coaddition results.

5.2.1 Five-year full-depth unWISE coadds

The mean integer coverage is 178 (177) frames per sky location in W1 (W2), roughly five times that of the AllWISE Atlas stacks. The minimum integer coverage is 65 (60) frames in W1 (W2) – there are no missing "holes" anywhere on the sky. The maximum integer coverage is 24,563 (24,514) frames in W1 (W2), occurring near the north ecliptic pole. Our coaddition computations did not require us to discard any usable data at the ecliptic poles.

5.2.2 Five-year time-resolved unWISE coadds

Each `coadd_id` tile footprint has at least 9 coadd epochs available per band. A median of 10 coadd epochs per band is available over the full sky. The maximum number of coadd epochs per band is 185, near the ecliptics poles. Figure 2 shows the spatial distribution of the number of coadd epochs per band. This distribution of the number of coadd epochs matches expectations based on the time periods during which WISE was/wasn't observing, the WISE survey geometry, and our time-slicing algorithm. Over the entire sky, the total number of single-band epochal coadds in the five-year unWISE data set is 387,915.

6 ASTROMETRIC RECALIBRATION TO GAIA DR2

6.1 Full-depth coadd astrometry

In previous work (Meisner et al. 2018d,c), we have presented a detailed characterization of the unWISE time-resolved coadd astrometry, along with refined WCS parameters designed to optimize the time-resolved coadds for proper motion studies. However, until now we have not provided such an astrometric analysis for our full-depth unWISE coadds, which are constructed by simply propagating the L1b WCS without modification. Making use of high-fidelity astrometry from the recently released Gaia DR2 (Gaia Collaboration et al. 2018), we present an assessment of the five-year full-depth unWISE coadd astrometry and describe our corresponding creation of improved WCS solutions. We obtain centroids of sources in the five-year unWISE stacks from the full-sky unWISE Catalog (Schlafly et al. 2019), which provides completely independent astrometric measurements in each of the W1 and W2 bands. The unWISE Catalog astrometry is based on model fits, and for the purposes of this analysis is equivalent to simple flux-weighted centroiding, since the unWISE Catalog PSF models are constructed so as to always place the flux-weighted centroid at the origin.

6.1.1 Computing per-coadd offsets relative to Gaia

We begin by computing per-coadd median astrometric offsets relative to Gaia for each full-depth coadd. Each full-depth coadd identified by its unique (`coadd_id`, band) pair is analyzed independently. We seek to compute median per-coadd offsets along the unWISE x and y pixel coordinate directions, and in RA and Dec. For each unWISE `coadd_id` footprint, we gather the list of Gaia DR2 sources that fall within this footprint and have full astrometric solutions available. This latter requirement is enforced because we wish to propagate the Gaia coordinates to the mean epoch of each unWISE coadd before performing any unWISE versus Gaia comparisons. We use the unWISE `-frames` table corresponding to each coadd to compute the mean MJD of the contributing frames. We then propagate Gaia positions to the mean epoch of each unWISE coadd based on the Gaia proper motions. We ignore parallax because the full-depth

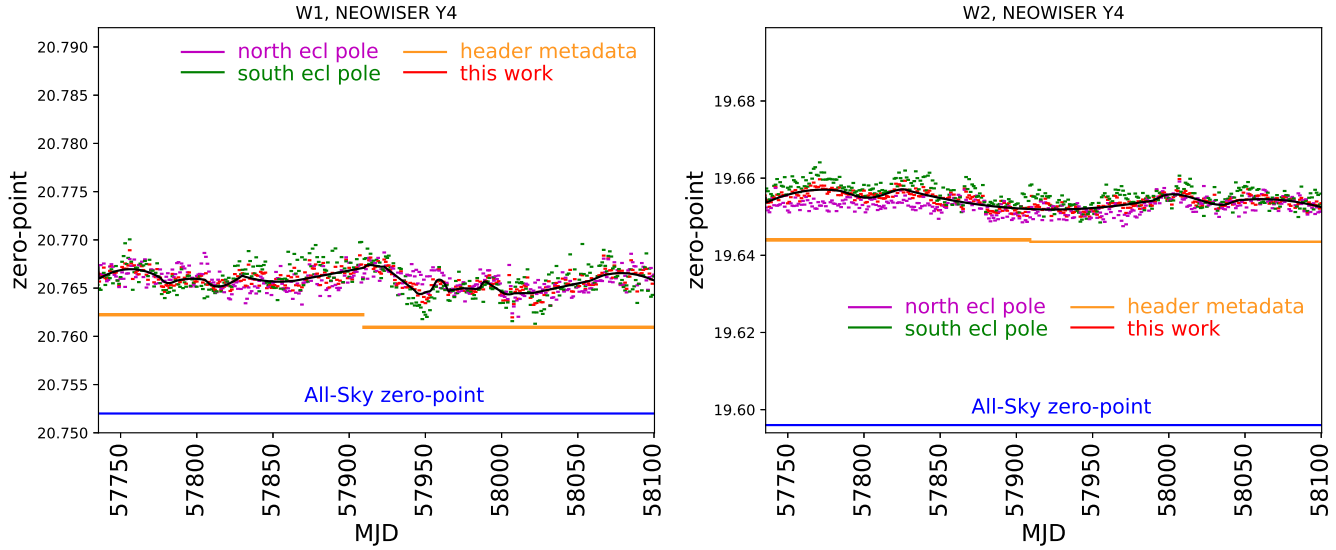

Figure 1. Custom photometric zero-points derived for the fourth year of NEOWISER data, as described in §4 of Meisner et al. (2017a). Left: W1. Right: W2. Our per-day zero-point measurements are shown as red dashes. Black lines show the smooth functions used to interpolate off of the per-day zero-point measurements during coaddition. There is no discontinuity in our derived zero-points at the boundary between the third and fourth year NEOWISER releases.

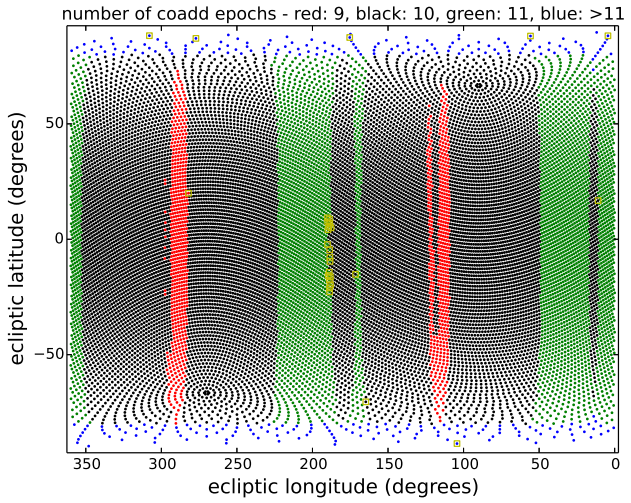

Figure 2. Number of W1 coadd epochs per `coadd_id` astrometric footprint, in ecliptic coordinates. Yellow boxes denote tiles for which the number of W1 coadd epochs differs from the number of W2 coadd epochs. Usually there are ten coadd epochs available per band (black dots). The red-colored ranges of ecliptic longitude have only nine coadd epochs per band because they were impacted by the WISE command timing anomaly in 2014 April. The green-colored ranges of ecliptic longitude have an extra eleventh epoch because they were observed during the partially complete third sky pass of the pre-hibernation WISE mission. The ecliptic poles ($|\beta| > 80°$) are blue, indicating >11 available coadd epochs in each band as a result of the modified time-slicing strategy employed in this region, which splits the available exposures into a series of ∼10 day intervals.

unWISE coadds average together equal amounts of imaging on opposite sides of the parallactic ellipse as a result of the WISE survey strategy. The typical mean epoch of the five-year full-depth unWISE coadds is MJD ≈ 56970 (year ≈ 2014.85), whereas Gaia DR2 natively reports positions at epoch 2015.5.

For each full-depth unWISE coadd, we match the unWISE and Gaia sources using a radius of 2″, and compute offsets $\Delta x = \mathrm{median}(x_{unwise} - x_{gaia})$, $\Delta y = \mathrm{median}(y_{unwise} - y_{gaia})$ in terms of unWISE pixel coordinates. We also compute $\Delta\alpha = \mathrm{median}((\alpha_{unwise} - \alpha_{gaia}) \times \cos(\delta_{gaia}))$ and $\Delta\delta = \mathrm{median}(\delta_{unwise} - \delta_{gaia})$. Figure 3 (4) shows a full-sky map of $\Delta\alpha$ ($\Delta\delta$) for W2, where the per-coadd values have been binned into $N_{side} = 16$ HEALPix maps which were then smoothed with a 5° Gaussian kernel. The median number of unWISE-Gaia matches per coadd is 17,600 (13,500) in W1 (W2), varying between ∼6,100 (4,900) at very high Galactic latitude and a maximum of ∼196,000 (174,000) toward the inner Galaxy.

The trends shown in Figures 3-4 mainly reflect Galactic rotation and the solar apex motion. This results from the fact that pre-hibernation L1b images were calibrated to 2MASS without a proper motion correction. As a result, our maps of $\Delta\alpha$ and $\Delta\delta$ look much like Figures 1[2] and 2[3] of the AllWISE explanatory supplement §V.2.b.ii (Cutri et al. 2013), albeit substantially reduced in amplitude because our full-depth coadds average together pre and post hibernation imaging, with post-reactivation L1b WCS determined in a way that does account for proper motion of the calibrator sources.

[2] http://wise2.ipac.caltech.edu/docs/release/allwise/expsup/figures/sec5_2biif1.png
[3] http://wise2.ipac.caltech.edu/docs/release/allwise/expsup/figures/sec5_2biif2.png

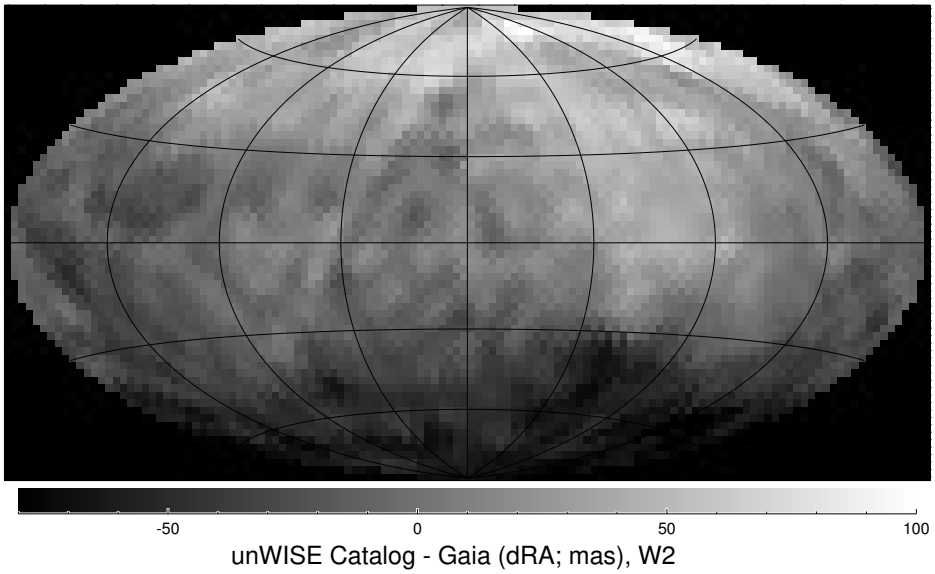

Figure 3. Full-sky map of five-year unWISE W2 full-depth $\Delta\alpha$ offsets relative to Gaia. The corresponding map for W1 looks similar.

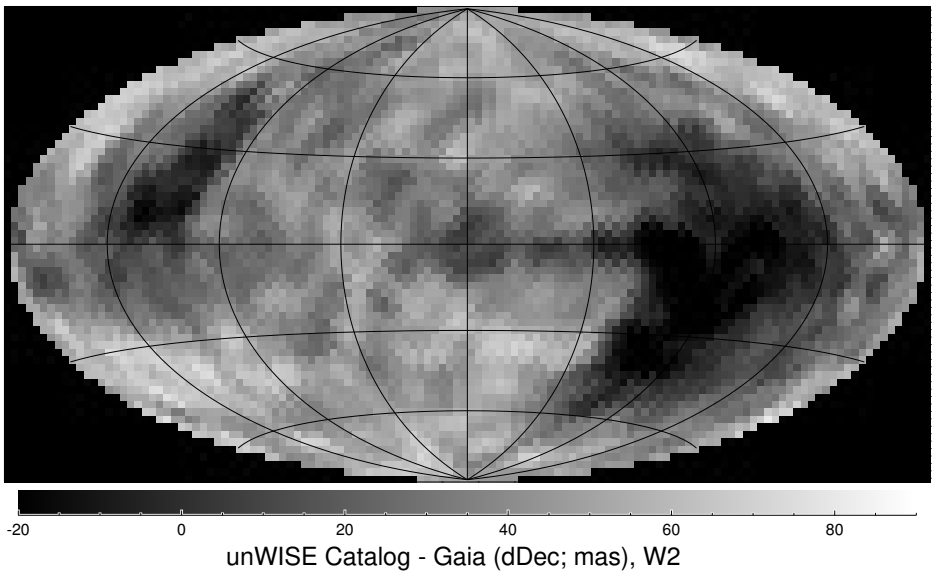

Figure 4. Full-sky map of five-year unWISE W2 full-depth $\Delta\delta$ offsets relative to Gaia. The corresponding map for W1 looks similar.

To provide a better sense for the behavior of the measured per-tile unWISE-Gaia offsets, Figure 5 shows plots of their trends in W2 as a function of Galactic latitude. $\Delta\alpha$ ramps between ~ -70 mas and $\sim +60$ mas, while $\Delta\delta$ mainly shows an overall offset of ~ 40 mas. Very similar trends are present in W1.

6.1.2 Recalibrated full-depth WCS

We use the per-coadd offsets Δx and Δy to create a full-sky set of 'recalibrated' WCS solutions for the five-year full-depth unWISE coadds. For each coadd identified by its unique (`coadd_id`, band) pair, we simply update the CRPIX reference pixel coordinates by assigning $\mathrm{CRPIX1}_{recalib} = \mathrm{CRPIX1}_0 + \Delta x$, $\mathrm{CRPIX2}_{recalib} = \mathrm{CRPIX2}_0 + \Delta y$. $\mathrm{CRPIX?}_{recalib}$ are the recalibrated CRPIX values, and $\mathrm{CRPIX?}_0$ are the original CRPIX values, which are always exactly 1024.5. We provide the updated WCS solutions in an index table called `fulldepth_neo4_index.fits`, which is meant to be analogous to unWISE index tables we have published previously containing recalibrated astrometry for our time-resolved coadds (Meisner et al. 2018d, Table 1). Table 1 provides column descriptions for the `fulldepth_neo4_index.fits` index table. In addition to the recalibrated WCS solution for each coadd, these contain related metadata such as the mean MJD values used to propagate Gaia positions to the unWISE epoch (`MJDMEAN`) and

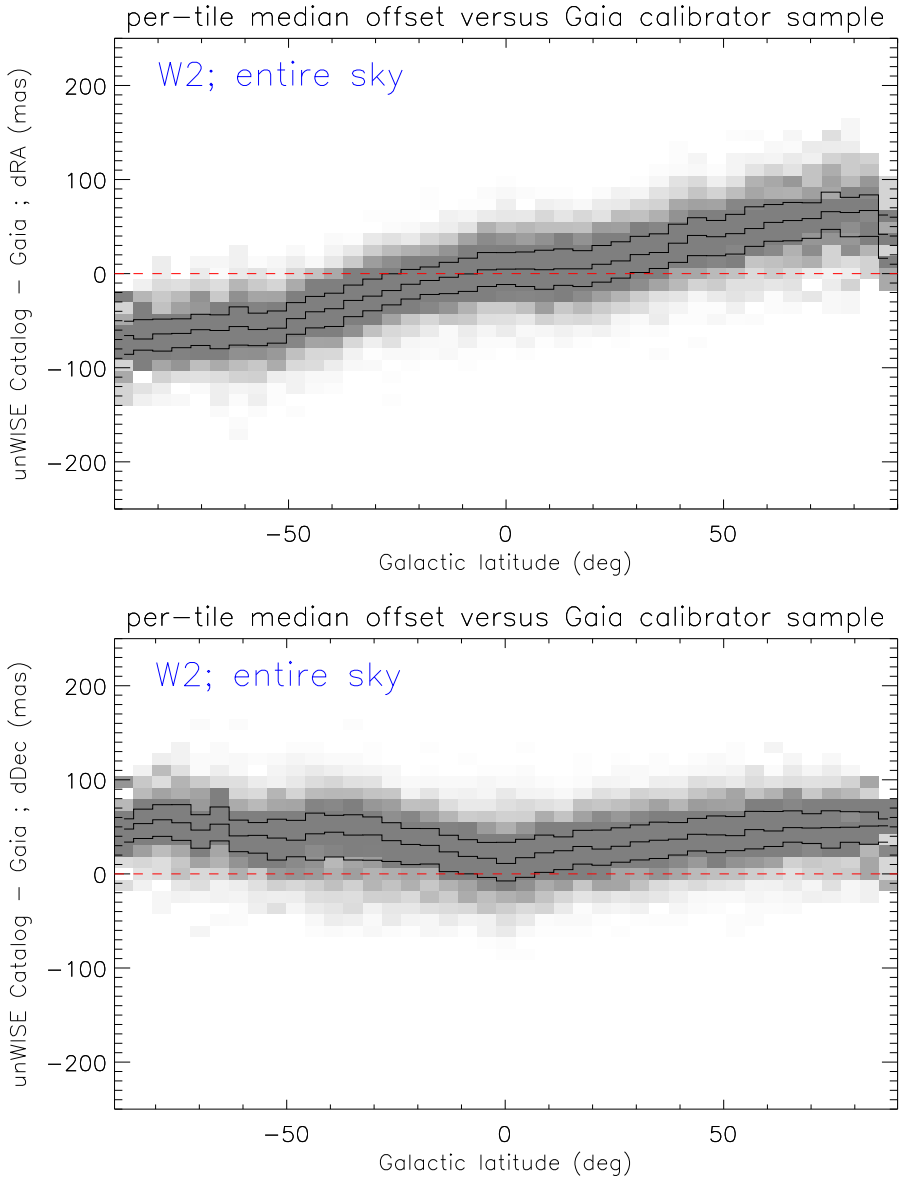

Figure 5. Trends of unWISE-Gaia per-tile offsets as a function of Galactic latitude, for W2.

the number of unWISE-matched Gaia astrometric calibration sources per coadd (`N_CALIB`).

6.1.3 Validation of recalibrated full-depth WCS

To verify that improved astrometry results from our recalibrated WCS solutions, we analyze a sample of spectroscopically confirmed quasars drawn from the SDSS "DR14Q" quasar catalog (Pâris et al. 2018). We downselect to quasars that have astrometry available from Gaia DR2, retaining DR14Q quasars with a Gaia counterpart within $2''$. ∼355,000 of ∼526,000 DR14Q quasars have such Gaia DR2 counterparts. Henceforward, for the DR14Q-Gaia sample of ∼355,000 quasars, we always adopt the Gaia DR2 positions. We match the DR14Q-Gaia quasar sample against the unWISE Catalog using a $2''$ radius, and compute per-object residuals in RA and Dec. The RA residuals include a multiplication by cos(Dec) so that they are in true angular units rather than being simple RA coordinate differences. Figure 6 plots the unWISE Catalog W1 quasar astrometry residuals as a function of Galactic latitude. As anticipated, these trends are similar to those shown for the per-tile unWISE-Gaia offsets in Figure 5, although we should not expect exactly the same trends given that the quasars sample a footprint which covers only ∼1/3 of the sky. Figure 7 shows the corresponding W1 quasar astrometry residuals using our recalibrated WCS solutions of §6.1.2. Figure 7 illustrates that systematic deviations of the quasar positions with respect to Gaia have been removed thanks to the recalibrated WCS solutions. Analogous plots of the W2 quasar astrometry residuals before and after recalibration show very similar results.

The Gaia-DR14Q quasars are not especially bright in WISE (median magnitudes of W1 ≈ 16.3, W2 ≈ 15.2), and their Gaia astrometry may contain excess scatter because

Table 1. Column descriptions for full-depth coadd recalibrated WCS index table.

Column	Description
COADD_ID	`coadd_id` astrometric footprint identifier
RA	tile center right ascension (degrees)
DEC	tile center declination (degrees)
BAND	integer WISE band; either 1 or 2
LGAL	Galactic longitude corresponding to tile center (degrees)
BGAL	Galactic latitude corresponding to tile center (degrees)
LAMBDA	ecliptic longitude corresponding to tile center (degrees)
BETA	ecliptic latitude corresponding to tile center (degrees)
MJDMIN	MJD value of earliest contributing exposure
MJDMAX	MJD value of latest contributing exposure
MJDMEAN	mean MJD of contributing exposures
DT	difference of MJDMAX and MJDMIN (days)
COVMIN	minimum integer coverage in unWISE `-n-u` coverage map
COVMAX	maximum integer coverage in unWISE `-n-u` coverage map
COVMED	median integer coverage in unWISE `-n-u` coverage map
N_EXP	number of exposures contributing to the coadd
N_CALIB	number of sources used for Gaia-based astrometric recalibration
NAXIS	2-elements NAXIS array for WCS
CD	2×2 CD matrix for WCS
CDELT	2-element CDELT array for WCS
CRPIX	2-element CRPIX array for WCS, incorporating Gaia-based corrections
CRVAL	2-element CRVAL array for WCS
CTYPE	2-element CTYPE array for WCS
LONGPOLE	LONGPOLE parameter for WCS
LATPOLE	LATPOLE parameter for WCS
PV2	2-element PV2 array for WCS

these objects have host galaxies which are likely often resolved by Gaia. Therefore, to gauge the bright end scatter of the unWISE astrometry after recalibration, we assemble a sample of "low-motion" stars in Gaia DR2, which are meant to be brighter analogs of our Gaia-DR14Q quasar sample. Specifically, we select Gaia DR2 sources with full astrometric solutions, `parallax` < 3 mas, `parallax_error` < 1 mas, $|$`pmra`$| < 1$ mas/yr, `pmra_error` < 1 mas/yr, $|$`pmdec`$| < 1$ mas/yr, and `pmdec_error` < 1 mas/yr. We then cross-match these Gaia sources to the unWISE Catalog with a radius of $2''$. We downselect to relatively WISE-bright sources which can still be confidently assumed unsaturated, with unWISE Catalog mags between 10 and 11.6 in the band under consideration. We further require $|b_{gal}| > 20^{\circ}$ and unWISE Catalog `fracflux` > 0.999. This results in Gaia-unWISE comparison samples of ∼17,000 (18,000) sources in W1 (W2). For these samples the median offsets before recalibration are −9 mas (−8 mas) in dRA in W1 (W2), and 29 mas (34 mas) in dDec. After recalibration, these median offsets are −1 mas (0 mas) in dRA in W1 (W2), and 0 mas (−2 mas) in dDec. In W1, the bright end scatter as measured by the robust RMS is 58 mas (45 mas) in dRA before (after) recalibration and 52 mas (42 mas) in dDec. In W2, the bright end scatter is 52 mas (37 mas) in dRA before (after) recalibration and 47 mas (36 mas) in dDec.

6.2 Time-resolved coadd astrometry

In Meisner et al. (2018d) we presented an extensive astrometric evaluation of the time-resolved unWISE coadds and showed that a bright end scatter of ∼40 mas per coordinate could be achieved with a coadd-level WCS recalibration following coaddition. That study was performed prior to the release of Gaia DR2, and hence we used the HSOY catalog (Altmann et al. 2017) to obtain calibrator sources with high-fidelity astrometry including proper motions that would allow us to propagate the calibrator coordinates to the epoch of each time-resolved coadd. For our five-year set of time-resolved coadds, we employ essentially the same astrometric recalibration procedure as in Meisner et al. (2018d), but we swap in the newly available Gaia DR2 for HSOY when obtaining calibrator sources. Here we provide updated astrometric recalibrations for all coadds using Gaia DR2, not just those coadds which are based on the most recently processed year of NEOWISE exposures.

For our sample of Gaia astrometric calibrators, we require a full 5-parameter astrometric solution so that proper motion is available for propagation of coordinates to each time-resolved coadd's epoch. The number of Gaia DR2 calibrators available per time-resolved coadd is typically ∼10-15% larger than the number previously available when using HSOY. For each of the 387,915 time-resolved coadds, we gathered the set of overlapping Gaia DR2 calibrators (typically ∼3,000-5,000 calibrator stars per tile footprint at high Galactic latitude) and propagated the Gaia coordinates to the relevant epoch. We then computed a first order SCAMP (Bertin 2006) solution for each coadd based on comparison of flux-weighted centroids measured from the time-resolved unWISE coadd against Gaia DR2 calibrator positions. Only 966 SCAMP recalibration failures occurred (representing just ∼0.25% of time-resolved coadds). We compared the SCAMP recalibrations using Gaia DR2 and HSOY for several hundred thousand coadds where we had both solutions available, and the results are extremely similar. The end re-

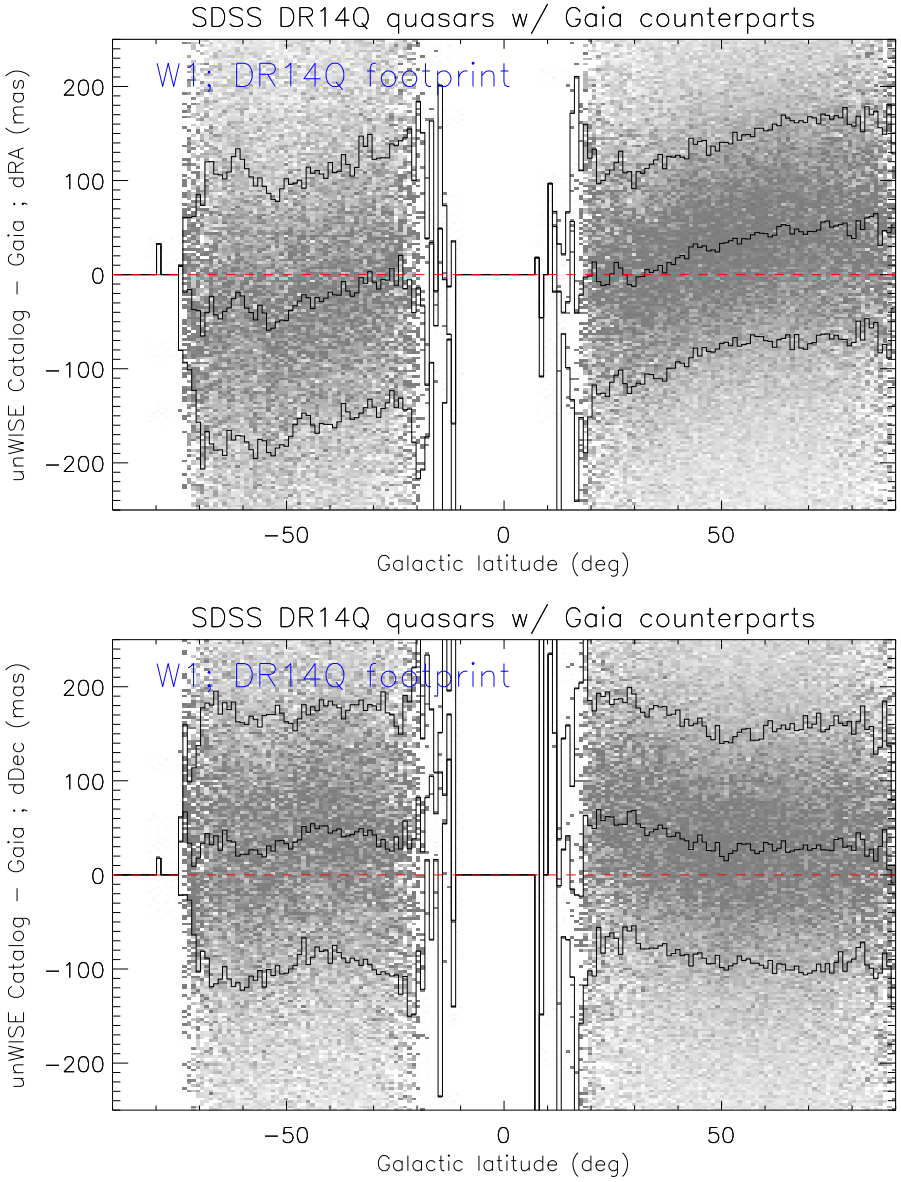

Figure 6. W1 unWISE Catalog astrometric residuals relative to Gaia as a function of Galactic latitude, for SDSS DR14Q spectroscopically confirmed quasars. As anticipated, the trends are similar to those of the per-coadd Gaia offsets shown in Figure 5, although we should not expect exactly the same trends given that the quasars sample a footprint which covers only ∼1/3 of the sky.

sult is as good as in (Meisner et al. 2018d): a ∼40 mas per coordinate bright-end scatter, which corresponds to ∼1/70 of a WISE pixel. The results of our time-resolved coadd WCS recalibrations are available as part of our five-year uWISE coadd data release (see §9 for details).

In this work we did not make use of the Gaia calibrator parallaxes when propagating Gaia coordinates to each time-resolved coadd's epoch, so our astrometric recalibrations do not provide absolute astrometry. Our typical Gaia DR2 calibrator source has a parallax of ∼1-1.5 mas, so we did not foresee any clearcut means to validate that a parallax correction had in fact been successful. In the future we will endeavor to incorporate Gaia parallaxes into our unWISE astrometric recalibration analyses.

7 OVERVIEW OF ARTIFACT FLAGGING ENHANCEMENTS

In Meisner et al. (2017b) we first introduced simplistic bright star masks to the set of unWISE coadd data products. These masks exist as a set of 18,240 images which together cover the entire sky. There is one unWISE bitmask image per unWISE tile footprint, combining artifact flagging information about the W1 and W2 bands into a single file. Currently, the unWISE bitmasks do not address the W3 or W4 bands, although extending them to do so is conceivable.

The original unWISE bitmasks from Meisner et al. (2017b) contained only four bits. As part of the present five-year unWISE coadd data release, we have dramatically enhanced the set of features now available in our unWISE bitmasks. The total number of mask bits has increased from

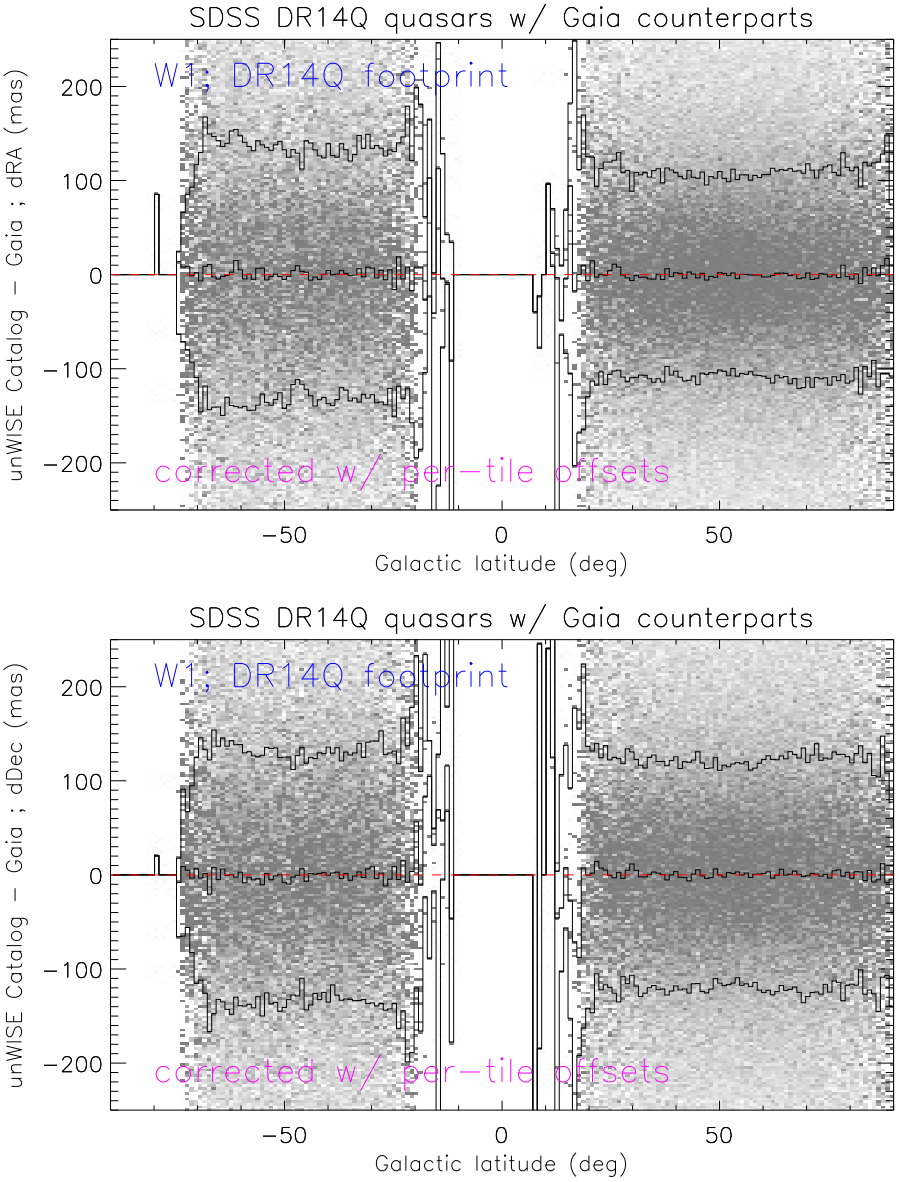

Figure 7. Residuals of recalibrated W1 unWISE positions relative to Gaia as a function of Galactic latitude, for SDSS DR14Q spectroscopically confirmed quasars. The systematic differences between unWISE and Gaia shown in Figure 6 have been removed.

4 to 31, and much more work has gone into ensuring that the masking behaves properly as a function of sky location (e.g., at low Galactic latitude and high ecliptic latitude).

The goal of the newly upgraded unWISE bitmasks is to provide a general purpose artifact flagging capability comparable to that of the WISE team's "CC flags", which were generated by a module called ARTID[4]. The unWISE bitmasks are also constructed with particular emphasis on enabling rare object searches ($\lesssim$ 1 per 500 deg^2). Most but not all of the unWISE mask bits are associated with artifacts from bright stars (see Table 2). The unWISE bitmasks are integer-valued and populated with sums of powers of 2, such that a particular bit can be isolated by taking the bitwise AND between the mask image and the desired power of 2. The mask bit definitions in Table 2 are also documented in the FITS header of each unWISE bitmask image. Appendix A fully explains the meanings of all mask bits, how the different bits are related to one another, and the detailed procedure for creating each unWISE mask bit. Our enhanced unWISE bitmasks are already in use by the unWISE Catalog (Schlafly et al. 2019), the DESI pre-imaging surveys (DR8 and onward; Dey et al. 2019), and the CatWISE motion catalog (Meisner et al. 2018b).

The unWISE bitmasks are optimized for catalogs that use detailed "pixelized" WISE PSF modeling and have a flexible WISE sky background model. To the extent that these capabilities are not implemented in a given WISE

[4] http://wise2.ipac.caltech.edu/docs/release/allsky/expsup/sec4_4g.html; ARTID computes flags at the catalog level and did not produce image-level renderings like those of the unWISE bitmasks.

Table 2. Definitions of unWISE artifact flagging mask bits.

Bit	Description
0	W1 bright star, southward scan
1	W1 bright star, northward scan
2	W2 bright star, southward scan
3	W2 bright star, northward scan
4	W1 bright star saturation
5	W2 bright star saturation
6	center of pixel not primary
7	W1 bright star, centroid off edge
8	W2 bright star, centroid off edge
9	resolved galaxy
10	big object (LMC, SMC, M31)
11	W2 optical ghost, southward scan
12	W2 optical ghost, northward scan
13	W1 first latent, southward scan
14	W1 first latent, northward scan
15	W2 first latent, southward scan
16	W2 first latent, northward scan
17	W1 second latent, southward scan
18	W1 second latent, northward scan
19	W2 second latent, southward scan
20	W2 second latent, northward scan
21	may contain W1 bright star centroid
22	may contain W2 bright star centroid
23	AllWISE-like W1 circular halo
24	AllWISE-like W2 circular halo
25	W1 optical ghost, southward scan
26	W1 optical ghost, northward scan
27	PSF-based W1 diffraction spike
28	PSF-based W2 diffraction spike
29	geometric W1 diffraction spike
30	geometric W2 diffraction spike

catalog's construction, the unWISE bitmasks may underflag features such as diffraction spikes and background level variations due to scattered light. Some artifacts are assigned separate unWISE mask bits for northward versus southward scan directions; this may be useful for time domain applications.The fraction of area flagged by any unWISE mask bit in either W1 or W2 ramps up from ∼1% at Galactic latitude of 90° to ∼5% at the lowest Galactic latitude edge of the extragalactic sky (as defined by the DESI cosmology survey footprint's boundary, $|b_{gal}| \sim 18°$).

8 VALIDATION OF FIVE-YEAR UNWISE COADDS

The improved depth of our five-year unWISE coadds can be readily discerned by comparing the pixel noise present in our new coadds versus those which only use pre-hibernation WISE data, such as the AllWISE Atlas stacks and the original Lang (2014) unWISE coadds. Figure 8 illustrates this decreased pixel noise, and hence increased depth, by showing side-by-side coadd cutouts in the COSMOS region, a typical area of extragalactic sky at low ecliptic latitude. Comparison of pixel value histograms for the 1 yr versus 5 yr unWISE stacks on the full COSMOS tile footprint (`coadd_id` = 1497p015) also shows that our new stacks have ∼2× tighter distributions, consistent with being ∼2× deeper in terms of their 5σ flux limit. Because the histograms are substantially skewed by the presence of compact sources, it is not ideal to use these in quoting a precise estimate for the depth improvement.

We have already presented a validation of the astrometric performance of our five-year unWISE coadds (§6), concluding that with recalibration to Gaia DR2, they display a bright-end scatter of just ∼40 mas per coordinate, equivalent to 1/70 of a WISE pixel.

The unWISE Catalog (Schlafly et al. 2019) is based on the same five-year unWISE coadds presented in this work, and so the excellent catalog-level photometric performance already demonstrated by Schlafly et al. (2019) can be considered a thorough validation of our new coadds. The Schlafly et al. (2019) Figure 4 comparison to Spitzer truth catalogs in the COSMOS region (Sanders et al. 2007) demonstrates that our new coadds support source detection to 0.76 (0.67) mag deeper than does pre-hibernation WISE data alone in W1 (W2) – indeed a ∼2× depth enhancement. (Schlafly et al. 2019) also shows that for unsaturated sources, the photometry based on our five-year coadds is linear with that of AllWISE to within ∼3% over a ∼9 mag range in source brightness. The unWISE Catalog displays overall photomeric zeropoint offsets relative to AllWISE of 4 mmag (32 mmag) in W1 (W2), but these could be due to choices made in normalizing the PSF models rather than anything related to the multiplicative scaling of the unWISE coadds themselves.

9 DATA RELEASE

The five-year unWISE coadd data release is publicly available online[5]. The data release consists of a set of FITS files organized into a directory structure. Within the top-level data release directory, a subdirectory called `fulldepth/` contains the all-sky set of five-year full-depth unWISE coadds. The full-depth coadd outputs for each `coadd_id` are contained within a directory named after that `coadd_id`, with an intermediate level of directories named after the first three digits of the `coadd_id`. For example, both bands of `coadd_id` = 1497p015 full-depth products are in `fulldepth/149/1497p015`. The unWISE bitmask files discussed in §7 and Appendix A are those with names ending in `-msk.fits.gz`.

The time-resolved coadds can be found in a series of top-level subdirectories `e000`, `e001`, ..., `e184`, where the trailing three digits encode the unWISE epoch number[6]. Analogous to the full-depth directory structure, epoch 0 of `coadd_id` = 1497p015 is in a directory called `e000/149/1497p015`.

The recalibrated WCS solutions described in §6 are provided in FITS binary tables named `tr_neo4_index.fits` and `fulldepth/fulldepth_neo4_index.fits`. The data model of the former is provided in Table 1 of Meisner et al. (2018d), and the latter's data model is specified in Table 1.

The total data volume of the five-year full-depth unWISE coadds is 2.9 TB. The total data volume of the five-year time-resolved unWISE coadds is 25.9 TB. The WiseView visualization tool (Caselden et al. 2018) provides a seamless browser-based interface for exploring cutouts and

[5] `https://faun.rc.fas.harvard.edu/ameisner/unwise/neo4`
[6] See §3.2.2 of Meisner et al. (2018d) for a precise definition of the unWISE time-resolved coadd epoch numbering scheme.

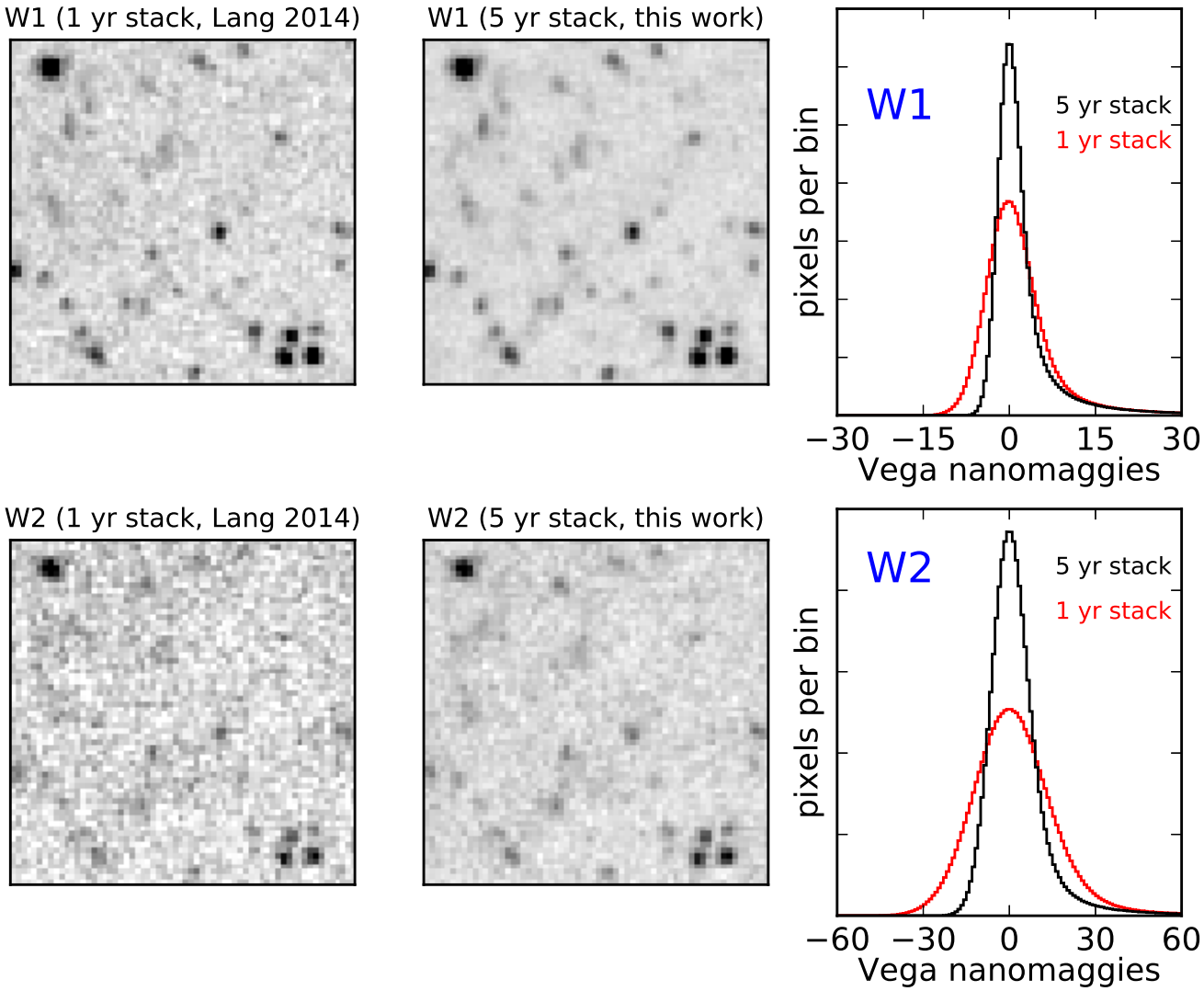

Figure 8. Illustration of the improved depth of the present W1/W2 coadds relative to those which only incorporate pre-hibernation WISE imaging. The top (bottom) row shows W1 (W2). Left column: Lang (2014) coadds. Center column: Corresponding coadds from this work. Cutouts are $2.9' \times 2.9'$, centered at $(\alpha, \delta) = (149.6155°, 1.4510°)$. Right column: Pixel value histograms for a $\sim$2.5 deg^2 region from which these cutouts have been drawn, indicating that a $\sim 2\times$ reduction in statistical noise has been achieved.

blinks of both the full-depth and time-resolved unWISE coadds without needing to download large volumes of coadded FITS images.

10 CONCLUSION

We have presented a new set of full-sky coadded maps based on the first five years of W1 and W2 imaging provided by the WISE and NEOWISE missions. Our new full-depth coadds now constitute the deepest ever all-sky maps at $3-5\mu$m, enabling detection of sources $\sim 2\times$ fainter than AllWISE at 5σ significance. Our full-sky set of time-resolved unWISE coadds provides a 7.5 year time baseline for measuring variability and motions of sources well below the single-exposure detection limit, a $15\times$ enhancement relative to the 0.5 year AllWISE time baseline. Relative to our prior (four-year) set of unWISE coadds, the full-depth stacks presented here provide a 25% increase in total exposure time and up to an 18% increase in the signal-to-noise of proper motion measurements. In addition to folding in an extra fifth year of NEOWISER imaging, we have also presented improvements to the coadd-level astrometric calibration and unWISE artifact flagging capabilities. The new image-level data products described in this work are already being used by several ambitious wide-area cataloging efforts: CatWISE, the unWISE Catalog, and the DESI pre-imaging surveys.

More archival analysis will be required to maximize the complete WISE/NEOWISE data set's value for Galactic and extragalactic astrophysics. A sixth year of W1/W2 imaging recently became publicly available in 2019 April, and these

new data ought to be incorporated into future versions of the unWISE coadds and derivative catalogs.

ACKNOWLEDGEMENTS

This work has been supported by grant NNH17AE75I from the NASA Astrophysics Data Analysis Program. We thank John Moustakas for sharing early versions of his LSLGA catalog with us.

This research makes use of data products from the Wide-field Infrared Survey Explorer, which is a joint project of the University of California, Los Angeles, and the Jet Propulsion Laboratory/California Institute of Technology, funded by the National Aeronautics and Space Administration. This research also makes use of data products from NEOWISE, which is a project of the Jet Propulsion Laboratory/California Institute of Technology, funded by the Planetary Science Division of the National Aeronautics and Space Administration. This research has made use of the NASA/ IPAC Infrared Science Archive, which is operated by the Jet Propulsion Laboratory, California Institute of Technology, under contract with the National Aeronautics and Space Administration.

The National Energy Research Scientific Computing Center, which is supported by the Office of Science of the U.S. Department of Energy under Contract No. DE-AC02-05CH11231, provided staff, computational resources, and data storage for this project.

REFERENCES

Altmann M., Roeser S., Demleitner M., Bastian U., Schilbach E., 2017, A&A, 600, L4
Bertin E., 2006, in Gabriel C., Arviset C., Ponz D., Enrique S., eds, Astronomical Society of the Pacific Conference Series Vol. 351, Astronomical Data Analysis Software and Systems XV. p. 112
Caselden D., Westin III P., Meisner A., Kuchner M., Colin G., 2018, WiseView: Visualizing motion and variability of faint WISE sources, Astrophysics Source Code Library (ascl:1806.004)
Cutri R. M., et al., 2013, Technical report, Explanatory Supplement to the AllWISE Data Release Products
Dey A., et al., 2019, AJ, 157, 168
Doré O., et al., 2018, arXiv e-prints, p. arXiv:1805.05489
Gaia Collaboration et al., 2018, A&A, 616, A1
Gardner J. P., et al., 2006, Space Sci. Rev., 123, 485
Kuchner M. J., et al., 2017, ApJ, 841, L19
Lang D., 2014, AJ, 147, 108
Lang D., Hogg D. W., Schlegel D., 2016, AJ, 151, 36
Mainzer A., et al., 2011, ApJ, 731, 53
Mainzer A., et al., 2014, ApJ, 792, 30
Mainzer A., et al., 2015, AJ, 149, 172
Makarov D., Prugniel P., Terekhova N., Courtois H., Vauglin I., 2014, A&A, 570, A13
Meisner A., Finkbeiner D. P., 2014, ApJ, 781, 5
Meisner A. M., Lang D., Schlegel D. J., 2017a, AJ, 153, 38
Meisner A., Lang D., Schlegel D., 2017b, AJ, 154, 161
Meisner A. M., Lang D., Schlegel D. J., 2018a, Research Notes of the American Astronomical Society, 2, 1
Meisner A., et al., 2018b, Research Notes of the American Astronomical Society, 2, 140
Meisner A. M., Lang D. A., Schlegel D. J., 2018c, Research Notes of the American Astronomical Society, 2, 202
Meisner A. M., Lang D., Schlegel D. J., 2018d, AJ, 156, 69
Pâris I., et al., 2018, A&A, 613, A51
Racca G. D., et al., 2016, in Space Telescopes and Instrumentation 2016: Optical, Infrared, and Millimeter Wave. p. 99040O (arXiv:1610.05508), doi:10.1117/12.2230762
Ross N. P., et al., 2018, MNRAS, 480, 4468
Sanders D. B., et al., 2007, ApJS, 172, 86
Schlafly E. F., et al., 2018, ApJS, 234, 39
Schlafly E. F., Meisner A. M., Green G. M., 2019, ApJS, 240, 30
Schlegel D. J., Finkbeiner D. P., Davis M., 1998, ApJ, 500, 525
Spergel D., et al., 2015, arXiv e-prints, p. arXiv:1503.03757
Stern D., et al., 2018, ApJ, 864, 27
Wheelock S. L., et al., 1994, NASA STI/Recon Technical Report N, 95
Wright E., Eisenhardt P., Mainzer A., Ressler M. E., Cutri R., Jarrett T., Kirkpatrick 2010, AJ, 140, 1868

APPENDIX A: COMPLETE UNWISE BITMASK DETAILS

This appendix provides full documentation of the mask bit meanings and methodology for our newly upgraded unWISE bitmask artifact flagging images.

A1 Bright source sample

A first step toward creating the unWISE bitmask images is defining a sample of sources which are sufficiently bright to potentially cause artifacts that require flagging. In Meisner et al. (2017b), we obtained such a sample via a simple full-sky query of the AllWISE catalog. Specifically, we selected all AllWISE sources with `w1mpro` < 9.5 (`w2mpro` < 8.3) in W1 (W2). We use Vega magnitudes and fluxes throughout this appendix unless otherwise noted. The equivalent thresholds in AB are 12.2 (11.64) in W1 (W2). Over the entire sky, this yields samples of 6,365,819 (2,221,020) sources in W1 (W2), with the density of such sources increasing dramatically near the Galactic plane. At $|b_{gal}| > 18^\circ$ (high enough Galactic latitude to fall within DESI's footprint), this bright source sample has on average $\sim$29 ($\sim$11) sources per deg^2 in W1 (W2).

Unfortunately, the AllWISE catalog lacks entries for some bright stars, and can report highly inaccurate (or "null") fluxes for some exceptionally bright objects that have far exceeded the WISE saturation threshold. To remedy this, the WISE team's ARTID artifact flagging module employed a custom "Bright Source List" that merged information from WISE itself, 2MASS, and even IRAS[7]. Here, we take a similar approach to enhancing our AllWISE-based bright source list, but using only 2MASS K_S magnitudes in a simplistic manner.

To merge 2MASS K_S information into our AllWISE-based bright source list, we begin by selecting all 68,661 2MASS sources with $K_S < 5$. We then cross-match this 2MASS K_S bright sample with our AllWISE sample, using a 15″ radius. This radius is chosen to allow for matching of stars with proper motions of up to $|\mu| \approx 1.5''$/yr

[7] http://wise2.ipac.caltech.edu/docs/release/allsky/expsup/sec4_4g.html#bright_source_list

given the ∼10 year AllWISE-2MASS time baseline. This proper motion threshold seems reasonable given that only ∼275 sources with $|\mu| > 1.5''$/yr are known, many of which (brown dwarfs, white dwarfs) are not sufficiently bright in W1 or W2 to require masking. For cases where an AllWISE bright source has a 2MASS $K_S < 5$ match within $15''$, we replace our bright source catalog's `w?mpro` magnitude with the 2MASS K_S magnitude, if $K_S <$ `w?mpro`. For 2MASS $K_S < 5$ sources with no AllWISE bright source match within $15''$ or a match at $>5''$ separation, we instantiate a new object in our WISE bright source list at the 2MASS object's position and with its `w?mpro` value set to the 2MASS K_S magnitude. In W1 (W2), 4,582 (877) bright sources have their WISE magnitudes replaced with 2MASS K_S, and an additional 2,767 (2,414) WISE bright source sample entries are instantiated based on 2MASS.

In the future we will investigate ways to more accurately predict W1 and W2 magnitudes of bright stars based on multi-band 2MASS JHK_S photometry, perhaps in combination with Gaia magnitudes and/or parallaxes. Also, given the availability of Gaia proper motions, improved 2MASS-AllWISE cross-matching could be enabled by propagating 2MASS positions to the AllWISE epoch. Lastly, unWISE coadds incorporate data spanning a considerable ∼8 year time period, so that one could imagine augmenting our WISE bright source list with motion information to instantiate multiple entries for bright sources that are moving very rapidly.

A2 PSF model thresholding

Many of the unWISE mask bits are generated via a method that we refer to as "PSF model thresholding": on each tile's footprint in each band, we render a model image containing only objects from our bright source sample, then produce binary masks by flagging model image pixels brighter than a specified threshold as being "contaminated". Figure A1 illustrates an example of this methodology. The W1 and W2 PSF models themselves are shown in the left column of Figure A2.

The key inputs to this procedure are the positions and fluxes from our bright source catalog (§A1), and the PSF model used to render the bright star profiles. For this purpose, we employ the Meisner & Finkbeiner (2014) W1 and W2 PSF models. These PSF models natively exist in WISE detector coordinates, so we must perform several modifications before applying them to render models of unWISE coadds. The Meisner & Finkbeiner (2014) PSFs include terms that account for PSF variation as a function of position within the detector. Because we wish to render models of unWISE coadd images that sample many detector positions at each bright source's location, we begin by constructing a PSF in each band that averages over detector position. We then use the world coordinate system of each coadd footprint to rotate the averaged PSF such that it has an orientation matching that of the detector on the sky. Typically there are two such rotations for each unWISE tile footprint, corresponding to northward and southward WISE scans — these two rotations of the PSF differ by 180° from one another. At very high ecliptic latitude, each bright star's location samples a substantial range of approach angles toward the ecliptic pole, meaning that the simple approximation of two discrete scan directions with PSF orientations separated by 180° no longer suffices. Currently, the unWISE mask bits constructed via PSF model thresholding do not account for this effect, which is only relevant over a very small fraction of the sky. With the PSF model averaged and rotated, for each bright source, we scale the PSF amplitude according to its magnitude listed in our bright source catalog and add it to the model image at the appropriate location. With the bright star model images in hand for each unWISE tile footprint, scan direction, and band we can proceed to apply various thresholding criteria, thereby flagging several types of artifacts. Full details of these thresholding steps are provided in subsequent sections.

One major limitation of the PSF model thresholding approach is that such flagging is limited in angular extent by the size of the PSF model. The Meisner & Finkbeiner (2014) W1/W2 PSFs extend quite far into the wings, with sidelengths of $14.9'$ (∼135 FWHM). Still, extremely bright stars can have diffraction spikes and "halos" reaching beyond the extent of our PSF models. Diffraction spikes become too long for the PSF models at parent magnitudes brighter than ∼ 4. At ∼ 0−0.5 mag, the circularly symmetric component of the PSF profile begins to extend beyond our PSF model. Therefore, we also produce geometric masks for diffraction spikes (§A14) and bright source circular halos (§A12), with radii that can extend far beyond the size of our PSF models.

A3 Bits 0-3: bright star 'core and wings'

Bits 0-3 are the original four mask bits from the Meisner et al. (2017b) unWISE bitmasks. They can be thought of as flagging the ∼0.6% (0.4%) of pixels most strongly affected by nearby bright source profiles in high Galactic latitude sky regions. These masks were originally created to identify areas affected by difference imaging artifacts. Thus, these bits may provide sufficient bright star masking for unWISE-based difference imaging analyses, or other analyses in which the PSF modeling yields residuals comparably good to those from difference imaging.

Having rendered our bright source only model as described in §A2 for the relevant band, scan direction and unWISE tile footprint, generating mask bits 0-3 amounts to simply thresholding on the model pixel values. Based on examination of typical extragalactic sky regions, we adopt the same baseline threshold in W1 and W2: $\Gamma_0 = 100$ nanomaggies per pixel. We then scale the brightness threshold (Γ) up with increasing source density, in attempt to avoid masking an excessive fraction of area at low Galactic latitude. To implement this scaling of Γ with source density, we begin by constructing a map of the number of Gaia DR2 (Gaia Collaboration et al. 2018) sources per $n_{side} = 32$ HEALPix pixel. We interpolate over the raw Gaia sources counts in HEALPix pixels affected by small-scale source density spikes (e.g., globular clusters) and localized dust clouds. We then interpolate off of the resulting source density map at coordinates corresponding to the center of the unWISE tile footprint for which we are constructing a bitmask, and refer to the resulting value as n_{src} (units of Gaia sources per $n_{side} = 32$ HEALPix pixel). The threshold Γ in nmgy/pixel as a function of source density is then determined by:

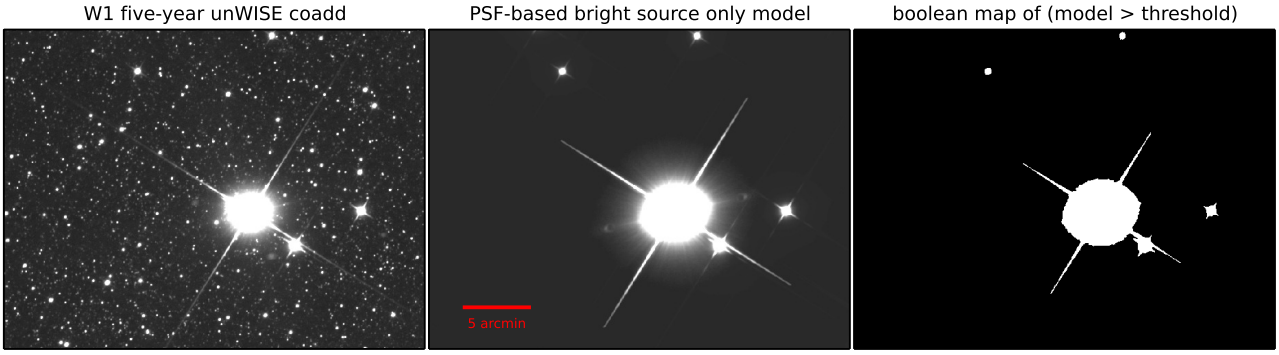

Figure A1. Schematic illustration of our PSF model thresholding procedure used in creating the unWISE bitmask images. Left: Portion of a five-year full-depth W1 unWISE coadd extracted from unWISE tile footprint 2415p106. The central, brightest source has AllWISE `w1mpro` ≈ 1.4. Middle: Bright source only model rendering of the same sky region, generated by combining the Meisner & Finkbeiner (2014) W1 PSF model, the unWISE coadd WCS, and our bright source list described in §A1. Right: Bright source only model thresholded at 100 Vega nanomaggies per pixel to create a boolean bitmask, as we do when generating unWISE mask bits 0 and 1. The white regions represent pixels flagged as contaminated by bright sources.

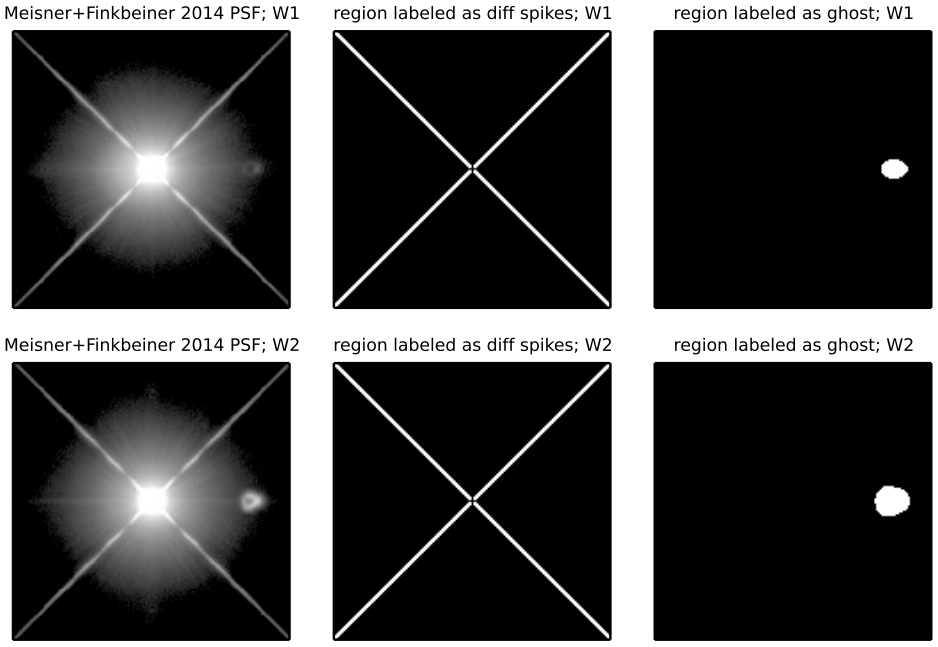

Figure A2. The PSF models used for creating our unWISE bitmasks, alongside corresponding boolean masks labeling PSF regions containing diffraction spikes and optical ghosts. Each subplot is 14.9′ on a side. Top left: W1 focal plane averaged PSF model. Top center: regions of the W1 PSF model labeled as containing diffraction spikes are shown in white on an otherwise black background. Top right: W1 PSF region labeled as being affected by an optical ghost. Bottom left: W2 focal plane averaged PSF model. Bottom center: regions of the W2 PSF model labeled as containing diffraction spikes. The top and bottom panels in the middle column are identical. Bottom right: W2 PSF region labeled as being affected by an optical ghost. The optical ghost is much more prominent in W2 than in W1.

$$\Gamma = \Gamma_0 + (max(n_{src}, 10^5) - 10^5) \times (\Gamma_{max} - \Gamma_0)/(n_{src,max} - 10^5) \quad \text{(A1)}$$

So the threshold ramps linearly from its minimum value of Γ_0 to its peak value of Γ_{max} between $n_{src} = 10^5$ and $n_{src} = n_{src,max}$. Γ remains at its baseline value so long as $n_{src} < 10^5$, which is the case for $\sim$75% of the sky. n_{max} is 3.1×10^6 Gaia sources per $n_{side} = 32$ HEALPix pixel. Γ_{max} is 10,000 nmgy/pixel (9250 nmgy/pixel) in W1 (W2).

Bit 0 (1) marks pixels which have values larger than Γ in the southward (northward) scan W1 model rendering. The same holds for bits 2 and 3 in W2. In constructing each of bits 0-3, we also dilate the binary map of pixels above threshold by a 3×3 square kernel. We refer to these bits as 'core and wings' because they capture the cores of bright star profiles, extending somewhat out into the wings so as to also capture diffraction spikes and optical ghosts for sufficiently bright objects. The most noticeable scan direction dependence seen in bits 0-3 pertains to the W2 ghost loca-

tion, appearing on opposite sides of the parent bright star in opposite scan directions.

Note that bits 0-3 mask regions containing the parent bright source centroids themselves. Also, bits 0-3 account properly for cases in which some portion of a parent bright source's PSF profile overlaps the tile under consideration despite the parent's centroid falling outside of the tile boundaries.

A4 Bits 4-5: bright source saturation

PSF modeling of bright sources will be compromised by inclusion of saturated pixels near the profile core. To address this, unWISE mask bit 4 (5) marks "saturated" pixels in W1 (W2). Pixels flagged by bit 4 (5) are the subset of pixels flagged by bright source bits 0 OR 1 (2 OR 3) with model profile values which exceed thresholds of 85,000 (130,000) Vega nanomaggies in W1 (W2). Note that these per-band thresholds are fixed across the entire sky, with no spatial variation.

For the purposes of these unWISE mask bits, we have not intended to define the "saturation" threshold such that it truly corresponds to saturation of the WISE detectors. Instead, we are masking pixels which may be either fully saturated, potentially non-linear, or be bright enough to experience non-linearities to due interactions with outlier rejection during unWISE coaddition. At high Galactic latitude, the fraction of area masked by bit 4 (5) is 4.3×10^{-5} (3.0×10^{-5}).

A5 Bit 6: center of pixel not primary

unWISE tile footprints are not mutually exclusive, and overlap by varying amounts depending on sky position. Typically, the overlap is $\sim3'$ along each boundary. As a result, one may sometimes wish to determine the "best" unWISE tile to consult for a specific (RA, Dec) sky location given the multiple tiles available to choose from. There are different possible ways to define "best". Here we define the best unWISE tile for a given (RA, Dec) as the tile which maximizes the minimum distance of that (RA, Dec) from any tile edge. For each pixel center's location within a given tile, one can compute whether this tile is the best tile for that pixel's (RA, Dec), or instead whether that sky location would be better analyzed in some other tile. Pixels marked with the "center of pixel not primary" unWISE mask bit are sky locations that would be better analyzed in another tile. The region flagged by this bit is a border along the edges of the tile, with a typical width of $\sim$35 pixels.

A6 Bits 7-8: contamination from bright source with centroid off tile edge

A bright source with PSF wings that contaminate an unWISE tile's footprint despite the bright source's centroid itself falling outside of the tile boundary can be problematic for image modeling analyses. For instance, the unWISE Catalog pipeline treats each unWISE tile footprint independently, detecting and modeling only those sources with centroids inside of the tile boundaries. As a result, the catalog creation process would by default be predisposed to model flux from the wings of off-edge bright sources as sums of large numbers of fainter point sources. To avoid this outcome, unWISE mask bits 7 and 8 flag pixels affected by bright stars with centroids outside of the tile's footprint. The unWISE Catalog pipeline recognizes these bits and uses them to preemptively make deblending less aggressive in the affected regions.

Bits 7-8 are based on bits 0-3 described in §A3. For W1, if bit 0 and/or bit 1 is set and the parent bright star centroid is off the tile edge, then bit 7 is also set. For W2, if bit 2 and/or bit 3 is set and the parent bright star centroid is off the tile edge, then bit 8 is also set. Because bit 7 (8) combines bits 0-1 (2-3) in W1 (W2), information about scan direction is not retained in bits 7-8.

A7 Bit 9: resolved galaxy

Certain image analyses may encounter problems in regions affected by resolved galaxies. For instance, the unWISE Catalog pipeline does not perform any galaxy model fitting, and by default deblends aggressively in attempt to explain all flux above background as a sum of point sources. Flagging of resolved galaxies allows unWISE Catalog deblending to be made less aggressive in these regions; this avoids shredding resolved galaxies into large numbers of point sources. For our purposes, resolved galaxies are those with sizes $\gtrsim 6.5''$, which is the approximate W1/W2 PSF FWHM.

To flag resolved galaxies, we use an early version of the Legacy Survey Large Galaxy Atlas[8] (LSLGA). This catalog contains $\sim$2.1 million galaxies with angular sizes of $d_{25} \gtrsim 7''$, a size threshold coincidentally well-matched to the WISE FWHM. We visually inspected the largest (in terms of angular size) 300 LSLGA galaxies, manually removing a small number of SDSS filter edge reflection artifacts and very low surface brightness dwarf galaxies, and also tweaking a few of the d_{25} parameters by eye. Based on this slightly modified LSLGA catalog, we used unWISE mask bit 9 to flag elliptical regions about each resolved galaxy, with the ellipse size set by d_{25} and the appropriate shape/orientation determined by the axis ratio and position angle. d_{25} is taken to be the major axis of the elliptical mask, as this visually appeared to work well. We masked circular regions in cases where position angles and/or axis ratios were not available. We also floored the b/a axis ratio at 0.5 to avoid overly line-like masked regions. The median per-tile fraction of area flagged by the resolved galaxy bit is 0.08%.

A8 Bit 10: big object

This mask bit was inspired by (and largely copied from) the `big_obj` mask bit within the (Schlegel et al. 1998, SFD) dust map data products. Its purpose is to flag regions affected by the LMC, SMC and M31. For the LMC and SMC, the unWISE big object mask bit is set for each pixel based on querying the SFD `big_obj` mask bit at that pixel center's (RA, Dec) coordinates. For M31, we use an elliptical mask with $a = 100'$, $a/b = 2.82$, and position angle of 35° east of north. This position angle was chosen in order to best cover M31's outskirts.

[8] https://github.com/moustakas/LSLGA. The LSLGA is based on HyperLeda (Makarov et al. 2014).

A9 Bits 11-12 and 25-26: optical ghost

Bright source ghosts are captured by the Meisner & Finkbeiner (2014) PSF models (see Figure A2). As a result, we can employ our PSF model thresholding approach in order to specially flag regions affected by ghosts, making use of the thresholding criterion defined in §A3. When rendering the same bright source only model used to create bits 0-3, we use the ghost regions labeled in the right column of Figure A2 to keep track of which pixels fall within bright source ghosts. We then generate our ghost-specific mask bits (11-12 in W2 and 25-26 in W1) by flagging those pixels that are within ghost-affected regions and have model surface brightnesses larger than $\Gamma_{ghost} = 0.15\Gamma$, where Γ is defined in Equation A1. In other words, we apply a *fainter* surface brightness threshold for masking within regions affected by ghosts, and assign the results of this modified thresholding to ghost-specific mask bits.

A10 Bits 13-20: latent

Persistence artifacts referred to as "latents" within the WISE documentation are present in W1 and W2 imaging. When a bright source is imaged and saturates one or more WISE pixels, the sky location imaged by those same detector pixels in subsequent exposures will display a diffuse blob-like latent feature. Latents are more pronounced in W1 than W2, and therefore tend to appear as somewhat blue smudges (see Figure A3). Exceptionally bright stars can cause latents that remain noticeable for many exposures while decaying in amplitude over time. We refer to the number of exposures since imaging of the parent bright source as the "order" of a latent. Currently, our unWISE masking accounts for only first and second order latents i.e., those arising one and two exposures subsequent to imaging of the parent bright source. Because WISE scans at $\sim$0.7° per exposure, the sky position of a latent is significantly offset from its parent source along the scan direction. This makes unflagged latents particularly troublesome for rare object searches — latents are difficult to trace back to their parent bright sources by eye, and can also be misinterpreted as flux variable or moving objects because they appear at different sky locations during different WISE sky passes which have differing scan directions. Latent positions are deterministic, and could all be predicted exactly given the WCS and timestamp of every exposure in combination with a perfectly accurate bright source catalog.

As a first step toward creating image-level unWISE latent masks, we generate a catalog of latents appearing in each unWISE tile footprint and each band. To make the computation of latent positions within each coadd efficient, we precompute per-band lookup tables containing the MJDs and full WCS parameters of all $\sim$25 million single-exposure W1/W2 images. For each unWISE tile footprint in each band, we use the unWISE `-frames` metadata table to determine the list of exposures contributing to the corresponding full-depth coadd. We then loop over these exposures, combining our WCS/MJD lookup table and bright source list (§A1) to determine the (RA, Dec) positions of latents appearing in each contributing exposure. We aggregate these latent world coordinates on a per-coadd basis, and convert this list of (RA, Dec) coordinates to pixel coordinates within the coadd under consideration. The result is one latent catalog per unWISE tile per band. In addition to world and coadd pixel coordinates, each such catalog contains a variety of metadata that will enable us to subsequently render image-level latent bitmasks. These metadata include, for each latent, the parent bright source magnitude, the WISE scan direction, and the latent's order (1 for first latent, 2 for second latent). In practice, when computing each coadd's catalog of latents, we do not analyze every single contributing exposure. Instead, we sort the contributing exposures by MJD and consider only every sixth exposure. This is done to reduce the computational cost of generating the latent catalog. Because a WISE sky pass typically includes $\gtrsim 12$ exposures at each sky location, and the WISE scan direction at a given sky position varies by $\lesssim 0.5°$ over the time period of six exposures, analyzing only the latents from every sixth exposure should not cause any image-level under-flagging downstream.

Table A1. Latent parent magnitude thresholds.

band	1^{st} latent threshold (mag)	2^{nd} latent threshold (mag)
W1	8.3	6.2
W2	7.0	4.9

Only a subset of the objects within our bright source list are sufficiently bright to create latents. Table A1 provides the magnitude thresholds that we employ for determining which bright sources are capable of causing first and second latents in each band. These thresholds are applied directly to the `w?mpro` values in our bright source list, and are taken to be constant over time and across the entire sky.

To determine the angular size of the region that should be masked around each single-exposure latent location, we define an effective parent magnitude ($m_{eff,l}$) that takes into account several factors: the parent bright source's magnitude, the ecliptic latitude and the background level. The following terms contribute to the determination of $m_{eff,l}$:

$$\Delta_{bg,l} = f_{bg,l} \cdot log_{10}\Big[max(intmed/intmed_0, 1)\Big] \qquad \text{(A2)}$$

$$\Delta_{arc,l} = 2.5 \cdot log_{10}(max(\delta\theta, \delta\theta_0)/\delta\theta_0),\ \ \delta\theta_0 = 1° \qquad \text{(A3)}$$

The effective parent magnitude used to compute the size of each single-exposure latent is then:

$$m_{eff,l} = m + \Delta_{bg,l} + \Delta_{arc,l} \qquad \text{(A4)}$$

Where m is the parent source's `w?mpro` value taken from our bright source list. *intmed* is the sky background level in WISE L1b DN. This sky background level is computed for each band on a per unWISE tile basis, by taking the median of the `intmedian` values in the unWISE `-frames` metadata table, restricted to frames that actually contributed to the coadd. The *intmed* value used in Equation A2 is that of the unWISE tile for which the bitmask image is being generated. $intmed_0$ is a fiducial background level appropriate at high Galactic latitude and low ecliptic latitude. In Equation A2, we adopt $intmed_0$ values of 25 (60) in W1 (W2). The $f_{bg,l}$ prefactor is set to 2.38 (3.78) in W1 (W2), and $\Delta_{bg,l}$ is capped at 4.3 magnitudes. We use $\Delta_{bg,l}$ to account for the

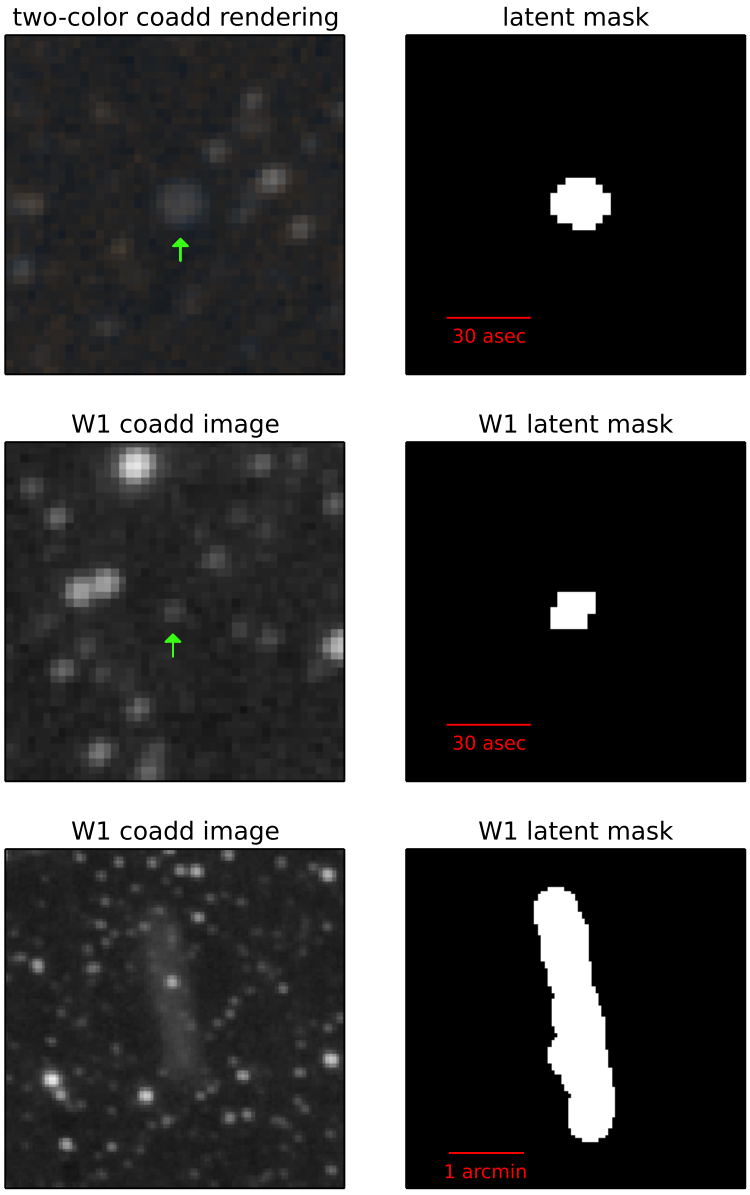

Figure A3. Examples of first order latents as imprinted on the unWISE coadds (left column) and flagged in our corresponding latent masks (right column). Top row: first latent of a $\sim$ 5th magnitude parent source, pointed to by a green arrow. The two-color composite at left displays W1 as blue and W2 as orange. This example illustrates the slightly blue appearance of latents relative to sources with typical color of W1$-$W2 $\approx$ 0. At right is a rendering of our unWISE bitmask in this latent's vicinity, with white pixels indicating that one or more of bits 13-16 is set. The location and size of the masked region match the observed artifact well. Middle row: W1 first latent of a `w1mpro` $\approx$ 8 parent source, which is close to the minimum brightness necessary to produce a latent. This latent covers a smaller region than does the first latent with $\sim$5th mag parent. Accordingly, a smaller region is flagged as affected by a W1 first latent, with white pixels at right indicating that bit 13 or 14 is set. Bottom row: latent arc produced by WISE scan direction variation at high absolute ecliptic latitude ($\beta \approx -76^\circ$). In this case the parent is a $\sim$ 2.5 mag star. The region flagged as affected by W1 first latents traces this arc, appearing to overflag somewhat as shown at right.

fact that an increased background level tends to reduce the region over which a latent's profile is non-negligible.

$\Delta_{arc,l}$ accounts for reduced latent surface brightness in the unWISE coadds due to increased arcing of latent imprints as $|\beta|$ becomes larger (see bottom row of Figure A3). Because of the continuous variation of the WISE scan direction at high ecliptic latitude, the coadd-level imprint of a bright source's multiple single-exposure latents is spread across an area which is $\sim \delta\theta/\delta\theta_0$ larger than it would have been in the ecliptic plane, with $\delta\theta$ given by:

$$\delta\theta = 0.78^\circ / cos(\beta) \tag{A5}$$

Equation A5 can be thought of as the range of ecliptic longitude spanned by a WISE exposure (0.78° on a side), as a function of ecliptic latitude. This approximately corre-

sponds to the range of ecliptic pole approach angles sampled as a function of β. $\delta\theta_0$ is set to 1° because this is the approximate ecliptic pole approach angle spread within a given scan parity (northward or southward) for regions near the ecliptic plane. We cap $\delta\theta$ at 180°, at which point latents will have been spread out into complete rings surrounding their parent stars[9]. Note that β in Equation A5 refers to the location of the parent bright source.

To flag pixels affected by latents in a given unWISE coadd footprint, we begin by using nearest neighbor interpolation to mark each pixel corresponding to a single-exposure latent listed in the relevant latent catalog and having $m_{eff,l} \leq m_{thresh}$, where m_{thresh} is the magnitude threshold for the type of latent being considered (see Table A1). We then apply a binary dilation about each of these marked pixels using a circular kernel, with a radius that depends on the difference $(m_{eff,l} - m_{thresh})$. Figure A4 shows the dilation radius in pixels as a function of $(m_{eff,l} - m_{thresh})$. We determined the shape of this function by assuming that for a parent source of magnitude m_{thresh}, only the centermost pixel of the profile is sufficiently saturated to yield a non-negligible latent imprint. Then, using the Meisner & Finkbeiner (2014) PSF model profile, we determined the radius of saturation that would result from making the total parent flux larger by $10^{-(m_{eff,l}-m_{thresh})/2.5}$.

As listed in Table 2, there are eight unWISE mask bits for latents, one for each possible combination of WISE band (W1 or W2), scan direction (north or south), and latent order (first or second). Currently, our latent masking is based on latent catalogs generated before we had incorporated 2MASS K_S information into our bright source list as described in §A1. In the future we will attempt to remedy this inconsistency with other unWISE mask bits by regenerating our latent catalogs based on the latest version of our bright source list. In future iterations of our latent catalogs, we may compute latents for every exposure as opposed to every sixth exposure despite the larger computational cost. Lastly, in future versions of our unWISE bitmasks, we may incorporate latents of exceptionally bright stars beyond second order.

A11 Bits 21-22: bright source centroid

Many unWISE mask bits associated with bright sources flag the location of the parent bright source itself, a feature which may at times be considered undesirable. To address this situation, mask bit 21 (22) marks a 3 × 3 pixel box surrounding the centroid of each object in the W1 (W2) bright source sample described in §A1.

A12 Bits 23-24: AllWISE-like circular bright source halo

In order to offer a set of unWISE mask bits similar to the AllWISE CC flags, we include bits flagging circular "halos" around bright sources. We attempt to use an AllWISE-like approach for creating our circular halo masks. Bit 23 (24) flags circular halos around bright sources in W1 (W2). Our halo radius formula, adapted from that of AllWISE, depends on the parent source's brightness, the sky background level, and absolute ecliptic latitude. The sky background level is relevant because the halos of bright stars become negligible at smaller radii when the sky background is higher, for example in the Galactic plane. The WISE coverage increases toward the ecliptic poles, so that for fixed parent star brightness and sky background level, the halo will tend to be appreciable relative to typical pixel noise out to a larger radius at higher absolute ecliptic latitude.

Table A2. Halo radius parameters.

band	a	b	c_{bg}	d_{bg}	B_{min}	B_{max}
W1	−0.144	3.134	−0.57	1.10	0.3	1.1
W2	−0.144	3.134	−1.35	2.30	0.3	1.1

To construct our sample of halo parent sources, we downselect the bright star sample of §A1 to sources with `w?mpro` < 8 in the relevant band[10]. We then use the following formulae to determine the halo radius, in arcseconds:

$$r_h = B \cdot 10^{a \cdot m_{eff,h} + b} \tag{A6}$$

$$B = c_{bg} \cdot log_{10}(intmed) + d_{bg}, \;\; B_{min} \leq B \leq B_{max} \tag{A7}$$

$$m_{eff,h} = m - 2.5 \cdot log_{10}\left[\sqrt{1/max[cos(\beta), 0.2]}\right] \tag{A8}$$

The parameters of these equations are provided in Table 2. m is the `w1mpro` (`w2mpro`) value from our bright source list for W1 (W2). β is ecliptic latitude. For each halo parent source, the *intmed* background level of the nearest tile center is adopted (see §A10 for a description of how per-tile *intmed* values are calculated). $m_{eff,h}$ is an "effective magnitude" appropriate for use in the halo radius computation given the values of the other parameters. $m_{eff,h}$ is brighter than m by an offset which tracks the signal-to-noise increase of a fixed flux source as its ecliptic latitude, and therefore WISE coverage, increases[11]. The halo radius parameters were tuned based on inspection of five-year "NEO4" unWISE coadds – different halo radii may be preferable when deeper or shallower unWISE coadds are being analyzed. Our halo radius functional forms and parameters are substantially rooted in those used by ARTID. Figure A5 shows our halo radii as a function of parent magnitude at $\beta = 0$ and with fiducial high Galactic latitude sky background levels.

At high Galactic latitude ($|b_{gal}| > 18°$), the typical fraction of area flagged by the unWISE circular halo masks is 1.2% (0.7%) in W1 (W2). We caution that circular masks are likely better implemented at the catalog level than at the image level, although image-level halo bitmasks do allow end

[9] This consideration is only relevant over a tiny portion of the sky, $|\beta| > 89.75°$.

[10] This requirement is an attempt to mirror the `w?mpro` < 8 cut documented in item vi.2 of `http://wise2.ipac.caltech.edu/docs/release/allsky/expsup/sec4_4g.html`.

[11] The WISE frame coverage scales like $1/\cos(\beta)$, only deviating from this trend very nearby the ecliptic poles.

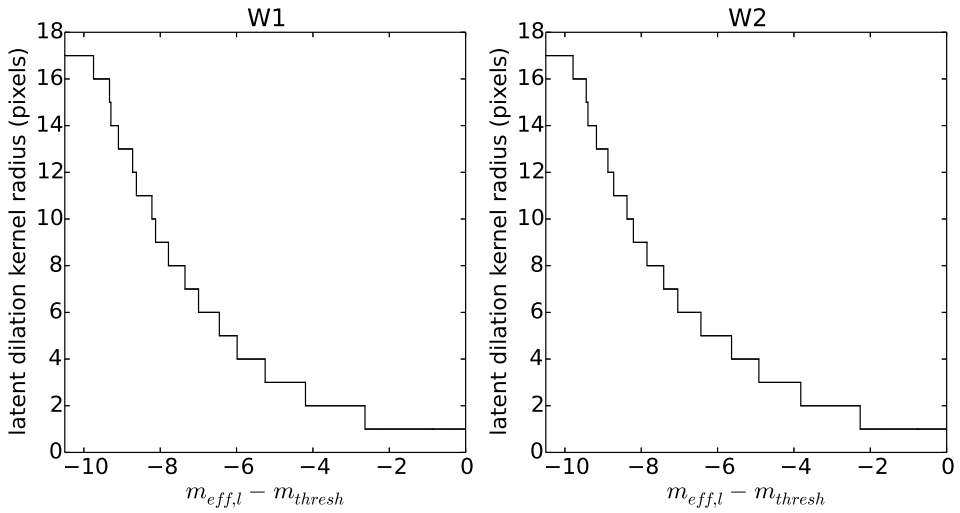

Figure A4. Radius of per-latent circular binary dilation kernel as a function of difference between the effective parent magnitude of the latent (Equation A4) and the latent parent magnitude threshold (Table A1). Left: W1. Right: W2. The radius is always floored at 1 pixel (corresponding to a 3×3 pixel rectangular dilation kernel), and capped at 17 pixels. For a given WISE band and order of latent, the region affected becomes larger as the parent's effective magnitude decreases. The increase of our adopted dilation radius toward lower $m_{eff,l}$ captures this behavior.

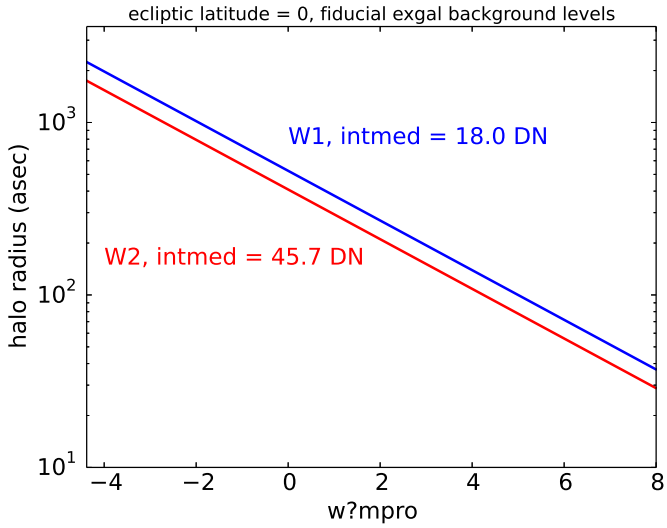

Figure A5. unWISE bitmask circular halo radii as a function of magnitude at $\beta = 0$ and with fiducial high Galactic latitude sky background levels.

users to conveniently dilate the halos as desired. Within each unWISE tile footprint, halos due to parent bright sources with centroids falling outside of the tile boundaries are always handled correctly.

A13 Bits 27-28: PSF-based diffraction spike

Given the spatial extent of the PSF models we employ, we can use our PSF thresholding approach to make "PSF-based" diffraction spike masks out to a radius of up to $\sim$10.5′. The methodology for doing so is analogous to that described in §A9 for generating ghost-specific mask bits. We track which pixels in our bright source only models are within diffraction spikes, based on the PSF regions labeled in the center column of Figure A2. Within these diffraction spike regions, we apply a reduced brightness threshold of $\Gamma_{spike} = 0.05\Gamma$, thereby generating mask bits specific to the diffraction spikes (bit 27 in W1 and 28 in W2). Because the WISE diffraction spikes are quite nearly symmetric under 180° rotation, the northward and southward scan direction diffraction spike masks are virtually identical. We therefore do not report PSF-based diffraction spikes using separate mask bits for each scan direction. Instead, each band's PSF-based diffraction spike bit is the OR of PSF-based diffraction spike flagging computed in the two scan directions.

A14 Bits 29-30: geometric diffraction spike

Diffraction spikes are captured to some extent in bits 0-3, and to a large extent in bits 27-28. However, for sufficiently bright stars, the diffraction spikes can reach beyond the boundaries of the Meisner & Finkbeiner (2014) W1/W2 PSF models, which are limited to $\sim$15′ on a side. To handle such situations, we have implemented geometric diffraction spike mask bits for `w?mpro` $\lesssim 6$ sources, extending up to $\sim$1° from the parent's centroid.

Our geometric diffraction spike masks consist of straight lines emanating outward from the bright source centroid at angles of 45°, 135°, 225°, and 315° from ecliptic north. In a manner similar to that used for determining circular halo size (§A12), we account for multiple factors when computing the geometric diffraction spike length: the parent source brightness, the sky background level, and the absolute ecliptic latitude. These factors are taken into account by computing an "effective magnitude" ($m_{eff,sp}$) for each object in our bright source sample. The following are terms that contribute to our computation of $m_{eff,sp}$:

$$\Delta_{bg,sp} = 2.5 \cdot log_{10}\left[max(intmed, intmed_0)/intmed_0\right] \quad \text{(A9)}$$

$$\Delta_{cov,sp} = -2.5 \cdot log_{10}\left[\sqrt{1/cos(min(\beta, 80°))}\right] \quad \text{(A10)}$$

The effective magnitude is then computed as:

$$m_{eff,sp} = m + \Delta_{bg,sp} + \Delta_{cov,sp} + \Delta_{fl,sp} \quad \text{(A11)}$$

Where m is the `w1mpro` (`w2mpro`) value from our bright source list in W1 (W2). We only generate geometric diffraction spike masks for bright sources with $m_{eff,sp} < 6$. $\Delta_{bg,sp}$ is a penalty that increases a bright source's magnitude (makes it considered to be effectively fainter) in regions of relatively high background. *intmed* is the sky background level in WISE L1b DN, defined the same way as in our latent effective magnitude computation. When computing geometric diffraction spike radii, we floor *intmed* at a fiducial extragalactic, low ecliptic latitude value $intmed_0$, taken to be 25 DN (60 DN) in W1 (W2). This forces $\Delta_{bg,sp}$ to be a strictly non-negative correction. $\Delta_{cov,sp}$ acts to decrease a bright source's effective magnitude (make it be considered brighter) with increasing absolute ecliptic latitude. At higher $|\beta|$, WISE provides larger frame coverage and hence reduced background noise in the unWISE coadds. The functional form of $\Delta_{bg,sp}$ results in a correction that tracks the decrease in background pixel noise with ecliptic latitude. In computing $\Delta_{bg,sp}$, we cap this ecliptic latitude correction at its $|\beta| = 80°$ value, to avoid applying excessively large corrections very nearby the ecliptic poles.

At high ecliptic latitude, each unWISE coadd averages together frames with a significant spread in approach angles toward the ecliptic pole. Diffraction spikes therefore begin to take on a "flared" appearance at high $|\beta|$, and are ultimately washed out into nearly disk-like patterns in the immediate vicinity of the ecliptic poles. This results in decreased diffraction spike surface brightness at high ecliptic latitude, which we account for with the $\Delta_{fl,sp}$ term in Equation A11. The value of $\Delta_{fl,sp}$ is given by the right hand side of Equation A3. In the case of geometric diffraction spikes, $\delta\theta$ (given by Equation A5) is capped at 90° because the flaring of diffraction spikes will form a complete "disk" around bright stars once the spread in ecliptic pole approach angles reaches this value (due to the fact that the single-exposure WISE diffraction spikes emanate outward at azimuthal angles spaced at 90° intervals).

Analytic functions of $m_{eff,sp}$ determine the geometric diffraction spike radius for each bright source. These functional forms and parameters are substantially rooted in those used by ARTID. The geometric diffraction spike radius is given by:

$$r_{sp} = B_L \cdot 10^{a_L \cdot max(m_{eff,sp}, -2) + b_L} \cdot T(m_{eff,sp}) \quad \text{(A12)}$$

$$T(m_{eff,sp}) = 1 - (6 - max(m_{eff,sp}, -2))/16 \quad \text{(A13)}$$

r_{sp} has units of arcseconds and $T(m_{eff,sp})$ is a tapering function that modulates the ARTID-like prescription in Equation A12. Given that Equation A13 floors $m_{eff,sp}$ at -2 and is only applied for $m_{eff,sp} < 6$, we always have $0.5 \leq T(m_{eff,sp}) < 1$. $T(m_{eff,sp})$ ramps linearly with effective magnitude in the range $-2 \leq m_{eff,sp} < 6$. The parameters of Equation A12 are listed in Table A3, and the geometric diffraction spike radius as a function of effective magnitude is shown in Figure A6.

Table A3. Geometric diffraction spike radius parameters.

band	B_L	a_L	b_L
W1	7.07	−0.195	3.38
W2	7.07	−0.178	3.14

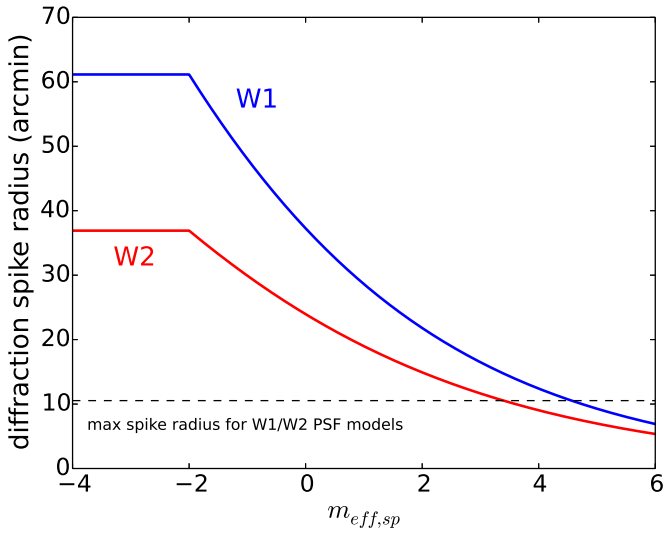

Figure A6. unWISE bitmask geometric diffraction spike radius as a function of effective magnitude, $m_{eff,sp}$. The blue (red) curve represents W1 (W2). The horizontal dashed black line is the maximum diffraction spike radius that can be accommodated within our PSF-based diffraction spike masking described in §A13. Our geometric diffraction spike masking goes into effect at $m_{eff,sp} = 6$, somewhat fainter than the effective magnitude at which the PSF-based diffraction spike masking can no longer be adequate ($m_{eff,sp} \approx 4$).

We initially mark geometric diffraction spikes as narrow, ∼1 pixel wide lines of the appropriate orientation and length. We then dilate these narrow versions of the geometric diffraction spike masks by an amount which depends on the parent bright source effective magnitude, dilating more aggressively for brighter parent sources. Specifically, we dilate with a 5 × 5 pixel square kernel for $m_{eff,sp} > 0$, a 9 × 9 pixel square kernel for $-2 < m_{eff,sp} \leq 0$, and a 13 × 13 pixel square kernel for $m_{eff,sp} \leq -2$.

Interior to each unWISE tile footprint, geometric diffraction spikes due to parent bright sources with centroids falling outside of the tile boundaries are handled correctly. Although we reduce the geometric diffraction spike radii to account for flaring at high $|\beta|$, this flaring is not reflected in the morphology of the regions masked. We hope to implement this functionality in a future release of the unWISE bitmasks; this limitation of the present bitmasks is only relevant over a small fraction of the sky near the ecliptic poles.

A15 Collapsing scheme for DESI pre-imaging and the unWISE Catalog

For certain applications, the full content of the native unWISE bitmasks (Table 2) may be unnecessary. In particular, the splitting of artifacts into multiple bits based on scan direction is only relevant for time domain applications. Several catalogs which do not require scan direction dependent masking information already employ our unWISE bitmasks. Specifically, these are the unWISE Catalog and the DESI pre-imaging surveys (Dey et al. 2019). For application to these catalogs, we have developed a scheme for collapsing the native 31-bit unWISE mask information into a smaller number of summary bits. The definitions of our 8 summary bits in terms of the native unWISE mask bits of Table 2 are provided in Table A4. The unWISE bitmasks are also being used by CatWISE, but with a different prescription for mapping the native unWISE mask bits to AllWISE-like character strings that encode the types of artifacts affecting each source.

A16 Other possible future bitmask improvements

In the preceding sections, we have suggested a number of detailed improvements we may implement in the future. In this section we mention a few additional upgrades that could be also be implemented.

- More finely pixelized bitmasks — The unWISE bitmasks are pixelized at the native WISE pixel scale of $2.75''$/pixel. Each such pixel covers an area equivalent to > 100 pixels of optical data from the DESI pre-imaging MzLS and DECaLS surveys. Thus, our current pixel size may limit the utility of applying our masks to WISE forced photometry based on detections in much higher resolution optical imaging. To address this, we could generate the unWISE bitmasks using a smaller pixel size.
- W3 and W4 — In the future we could include information about W3 and W4 in our unWISE bitmask products.
- Nebulosity — Nebulosity due to Galactic dust can be problematic for source detection and modeling analyses. The unWISE Catalog processing uses a neural network to classify whether or not a sky region is affected by nebulosity (Schlafly et al. 2018), and reports this information via the `flags_info` image product. This nebulosity flagging could potentially be added into the main unWISE bitmask images.
- Overflagging in the Galactic plane — Despite our efforts to limit masking in high source density regions, some mask bits still flag excessively large fractions of area in parts of the Galactic plane, mostly toward the Galactic center. Further tuning of the ways in which masking is scaled based on source density and sky background level could be attempted.
- Homogenizing procedures for different mask bits — More work could be done to homogenize the separate procedures used to create different unWISE mask bits. For example, our PSF thresholding scales back masking in crowded regions based on a map of Gaia source density, whereas the geometric and latent mask bits do so based on sky background level.

Table A4. Collapsing of unWISE mask bits for DESI pre-imaging and the unWISE Catalog.

Summary Bit	meaning	native unWISE bit logic (W1)	native unWISE bit logic (W2)
0	bright star core and wings	0 OR 1	2 OR 3
1	PSF-based diffraction spike	27	28
2	optical ghost	25 OR 26	11 OR 12
3	first latent	13 OR 14	15 OR 16
4	second latent	17 OR 18	19 OR 20
5	AllWISE-like circular halo	23	24
6	bright star saturation	4	5
7	geometric diffraction spike	29	30